CHAPTER IV

RESULTS AND DISCUSSION

This chapter describes experimental results related to the carbon nanotube modified glassy carbon (CNT/GC) and bismuth–CNT composite modified glassy carbon (Bi–CNT/GC) electrodes. Morphological information of CNTs and Bi–CNT composites were obtained. In addition, all of the modified electrodes were discussed in terms of their responses (peak heights) for the determination of cadmium (II) and lead (II) ions.

4.1 Purification and Modification of CNTs

Fourier transform infrared (FTIR) spectroscopy, X-ray diffraction (XRD) technique, and transmission electron microscopy (TEM) were employed to investigate the information about the CNT functional groups, which were generated from the oxidation of raw CNTs by concentrated acid. Data were directly compared between the modified and unmodified CNTs.

4.1.1 Fourier Transform Infrared (FTIR) Spectroscopic Analysis

Since the surfaces of raw CNTs are very hydrophobic, CNTs are unfavorable for metal deposition. Hence, the modification of CNT surfaces with functional groups is essential. FTIR spectra of the unmodified and modified CNTs are illustrated in Fig. 4.1. In both cases, the peaks at approximately 3420 and 1630 cm^{-1} can be attributed to vibrational modes of hydroxyl (–OH) and carbonyl (C=O) groups [47]. After the modification of CNTs with concentrated acid, FTIR spectrum of the modified CNTs (Fig. 4.1b) shows additional peaks at the wavenumbers of 1200 and 1720 cm^{-1}, representing the stretching vibrations of C–O and –COOH, respectively [48]. These FTIR results demonstrated that this acid treatment can generate the hydrophilic functional groups that improve the solubility of CNTs in aqueous media and promote metal–CNT interaction [49].

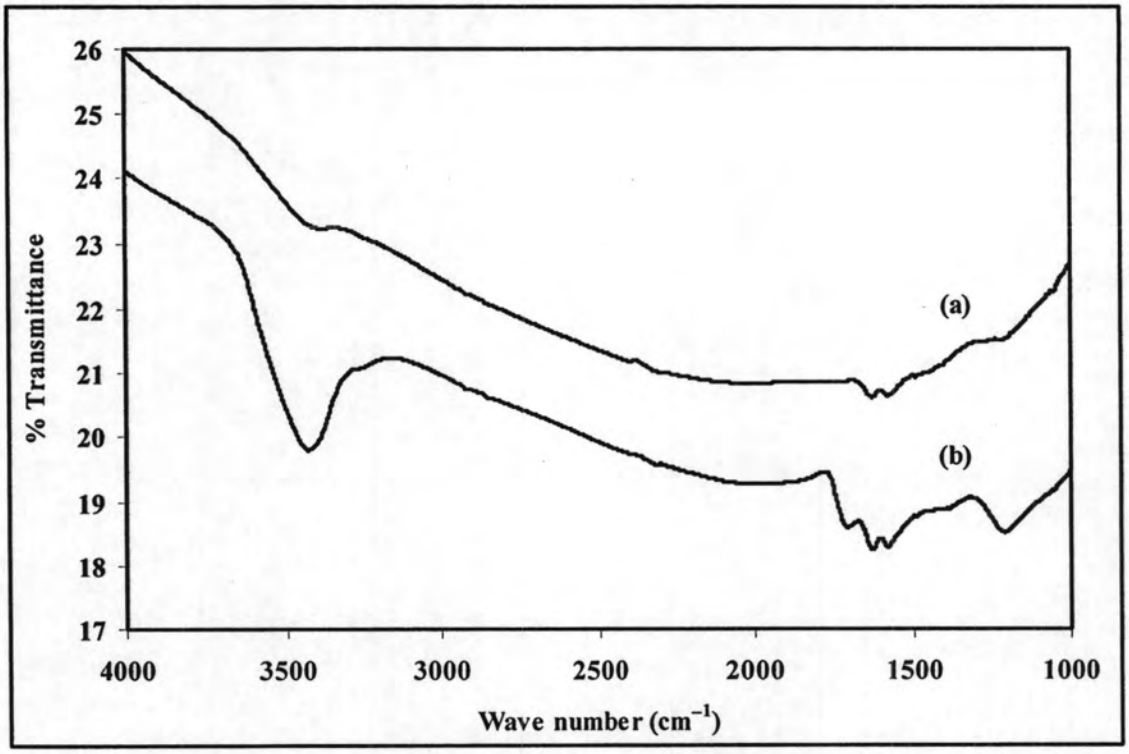

Figure 4.1 FTIR spectra of the (a) unmodified and (b) modified CNTs.

4.1.2 X-ray Diffraction (XRD) Analysis

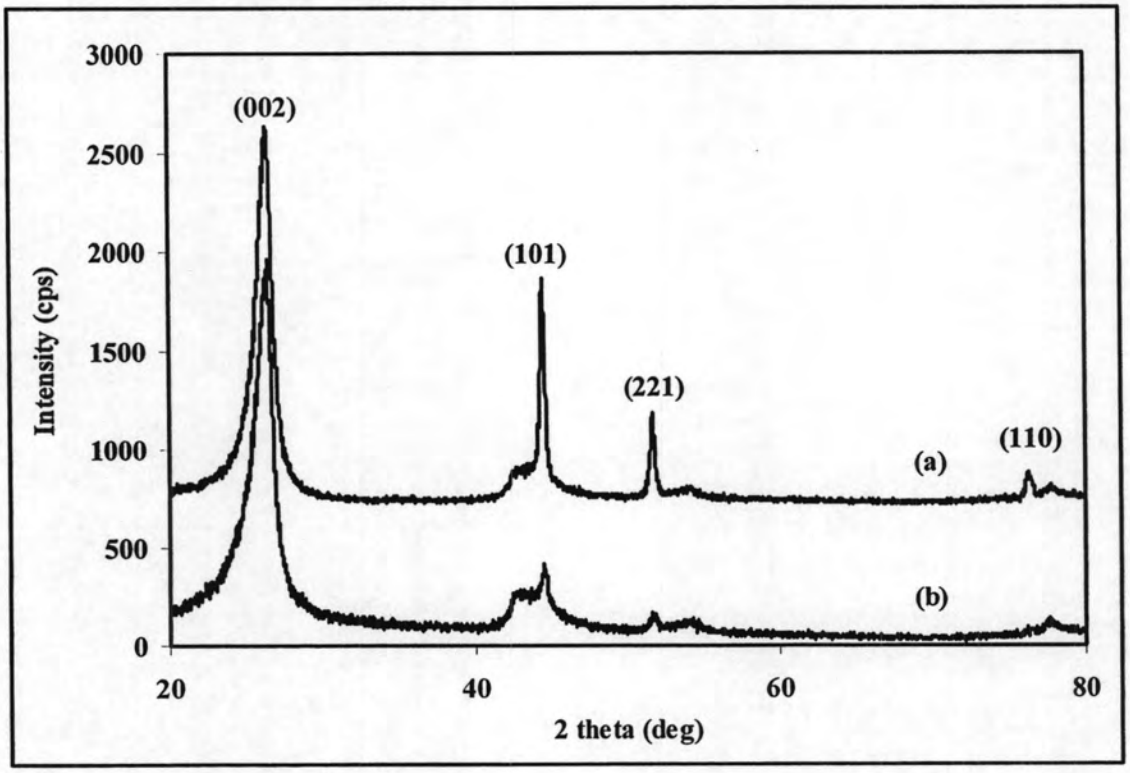

Figure 4.2 XRD patterns of the (a) unmodified and (b) modified CNTs.

Fig. 4.2 exhibits XRD patterns of the unmodified and modified CNTs observed at room temperature. For both types of CNTs, the XRD peaks at 26.30 degrees can be attributed to CNT (002). As displayed in Fig. 4.2a for the XRD pattern of the unmodified CNTs, the peak at approximately 44.42 degrees reflects the diffraction peak of residual nickel (101) whereas the diffraction peaks at 51.74 and 76.34 degrees represent graphite (221) and graphite (110), respectively [50]. XRD pattern of the modified CNTs (Fig. 4.2b) demonstrates the peaks at 44.38, 51.84, and 76.38 degrees with less intensities, revealing that the quantity of graphite and nickel residue can be reduced by the concentrated-acid treatment. These XRD results are in agreement with earlier literatures [51].

4.1.3 Transmission Electron Microscopic (TEM) Analysis

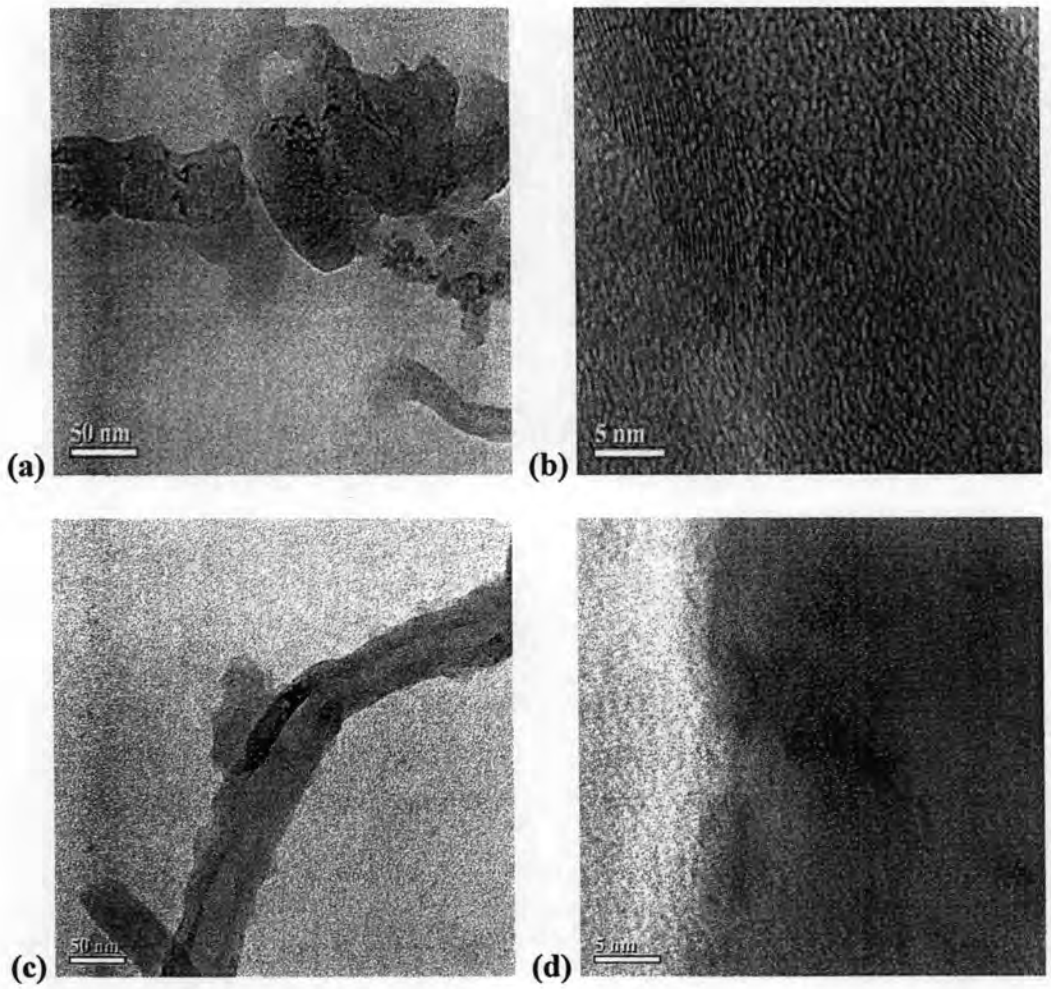

Figure 4.3 TEM images of the unmodified CNTs ((a) and (b)) and modified CNTs ((c) and (d)).

Fig. 4.3 compares TEM images of the unmodified and modified CNTs. It can be clearly seen from Fig. 4.3a and 4.3b that there are a lot of dark spots dispersing along the CNT tubes. These spots can be interpreted as impurities on the outer walls of unmodified CNTs. The impurities could be either an amorphous carbon generated as a side product during the CNT formation or the trace amount of nickel coming from the nickel nanoparticles used as the catalyst for the CNT synthesis. TEM images of the CNTs after the acid treatment (Fig. 4.3c and 4.3d) illustrate less amounts of the dark spots, revealing that, the impurities could be removed from the outer walls of CNTs. However, the presence of a few dark spots at the inside of the nanotubes have confirmed that tiny portion of impurities could not be removed, implying the inaccessibility of acid solution inside the nanotubes during the acid treatment. Note that it is possible to draw the same conclusion from XRD (Fig. 4.2) and TEM (Fig. 4.3) results that there are few impurities remained after the acid treatment.

4.2 Morphological Information of Bi–CNT Composites

Synthesized Bi–CNT composites were characterized by XRD technique, TEM, and energy dispersive X-ray fluorescence (EDXRF) spectrometry.

4.2.1 X-Ray Diffraction (XRD) Analysis

Fig. 4.4 displays XRD patterns of the synthesized Bi–CNT composites containing 1.00-32.00 mol % of bismuth *versus* 100 mol % of CNTs. In this report, these composites will be named as 1.00-32.00 mol % Bi–CNT composites. The diffraction peak at $2\theta = 24.5°$ correspond to the plane (002) of graphite [52], indicating the presence of CNTs. While the other diffraction peaks in Fig. 4.4 represent the planes of bismuth [53]. This result exhibited the successful deposition of bismuth onto CNTs. It is important to point out that 12.00 $g \cdot mol^{-1}$ has been used as a formula weight of CNT.

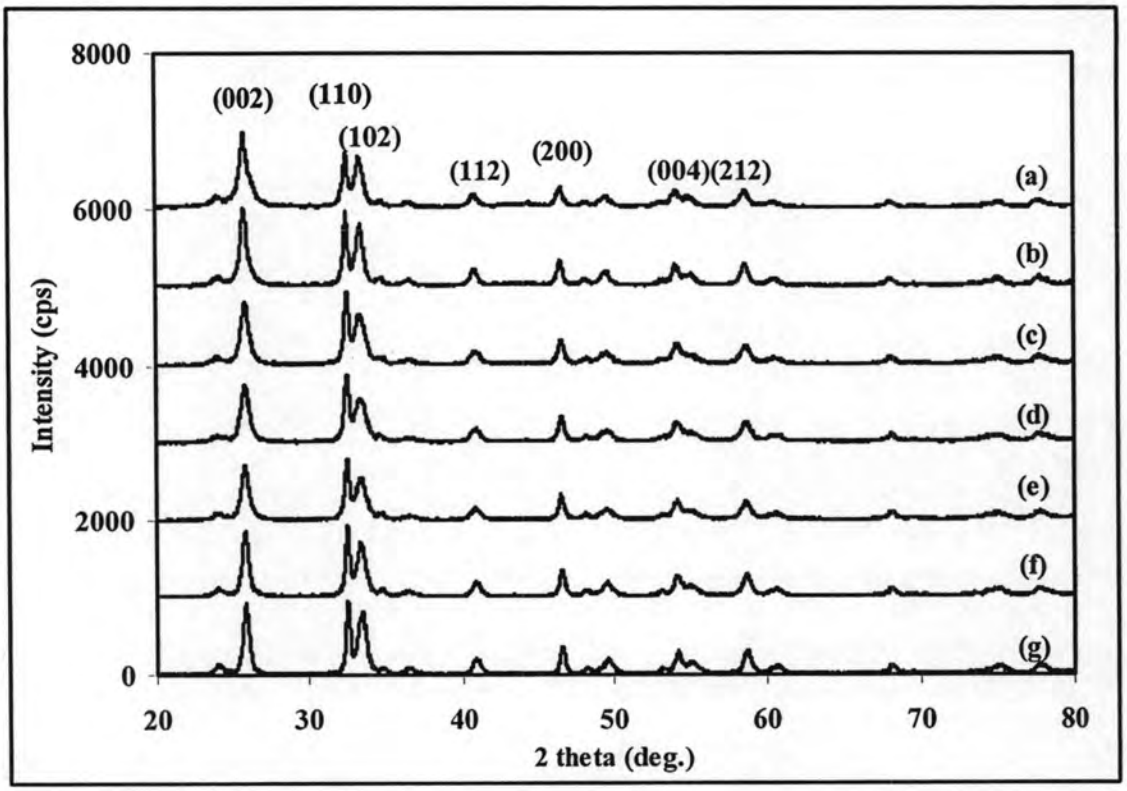

Figure 4.4 XRD patterns of (a) 1.00, (b) 2.00, (c) 4.00, (d) 6.00, (e) 8.00, (f) 16.00, and (g) 32.00 mol % Bi–CNT composites.

4.2.2 Transmission Electron Microscopic (TEM) Analysis

As the representative of Bi–CNT composites, TEM images of 4.00 mol % Bi–CNT composite with different magnification powers are displayed in Fig. 4.5. Similar to TEM images of CNTs (Fig. 4.3), the dark spots superimposed on the long-chain nanotubes are likely to be small particles deposited on CNTs. In combination with XRD evidence (Fig. 4.4), it can be explained that small bismuth particles were distributed on the surface of CNTs. Well dispersion of the Bi–CNT composite without further agglomeration was observed for this composite. The average size of the Bi–CNT composite is approximately 50 nm. This is the first report illustrating the successful preparation of Bi–CNT composites.

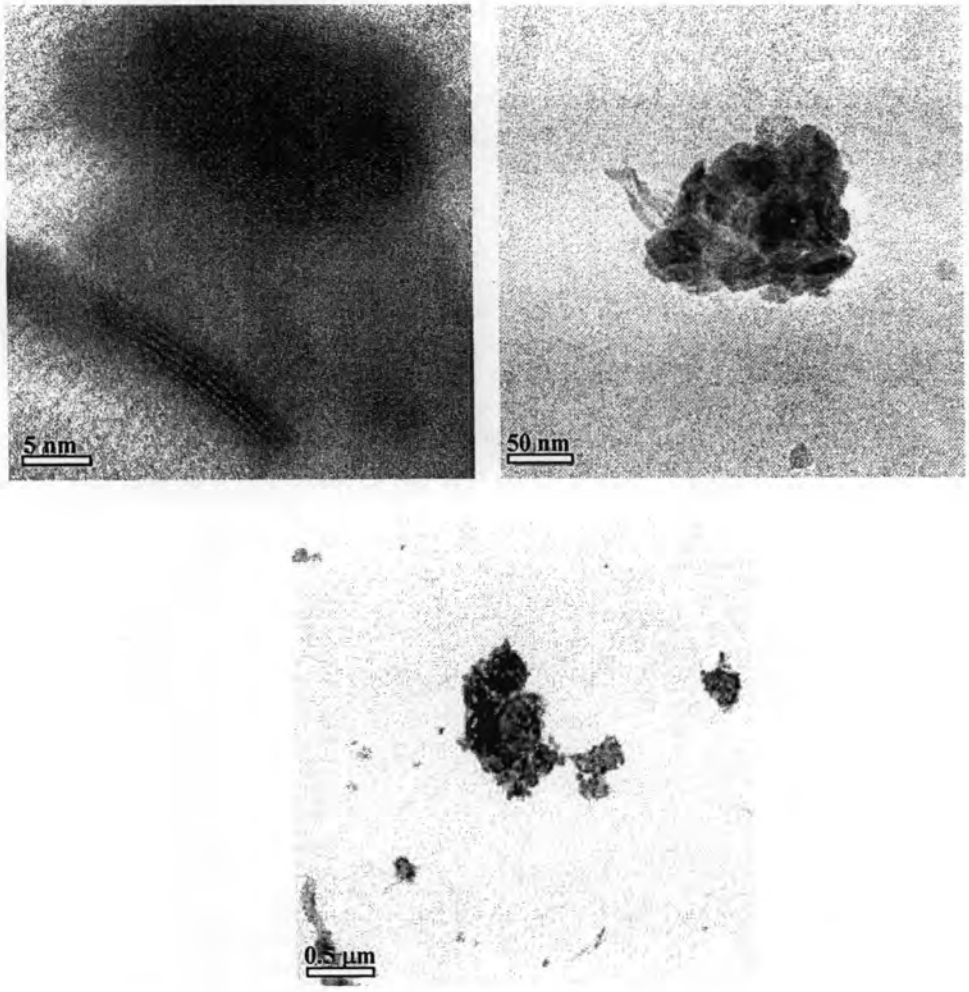

Figure 4.5 TEM images of 4.00 mol % Bi–CNT composite.

4.2.3 Energy Dispersive X-ray Fluorescence (EDXRF) Spectroscopic Analysis

In this work, EDXRF measurement was selected to determine the actual composition of Bi–CNT composites. Table 4.1 demonstrates mol % of bismuth in Bi–CNT composites, showing the quantities of bismuth precursor added for the synthesis and the actual quantities of bismuth in the obtained composites. It is evident that bismuth was presented with the CNT support, indicating that $Bi(NO_3)_3 \cdot 5H_2O$ precursor can successfully be reduced onto CNT surfaces by ethylene glycol ($HO(CH_2)_2OH$). EDXRF of Bi–CNT composites with 4.00-32.00 mol % of bismuth precursor indicated that, setting moles of CNTs as 100%, the actual amount of bismuth on CNTs maintained at approximately 2.00-3.00 mol % of bismuth. These results might be because CNTs had limited active sites for the electrodeposition of

bismuth. Therefore, the mole percentages of bismuth in Bi–CNT composites were less than the amounts of bismuth added in the synthesis. Similar result had been demonstrated in the preparation of copper supported on CNTs. For the deposition of 10.00 wt. % copper onto CNTs by polyol process, the actual copper content on CNTs was 7.20 wt. % [54].

Table 4.1 Mole percentage of bismuth in Bi–CNT composites.

Mol % of Bismuth in Bi–CNT Composites[a]	
% Calculated from Bismuth Precursor[b]	Actual % Obtained from EDXRF Measurement
1.00	1.18
2.00	1.78
4.00	2.00
6.00	2.07
8.00	2.53
16.00	3.06
32.00	2.31

[a] CNTs were set as 100% in all composites.

[b] 12.00 $g \cdot mol^{-1}$ was used as the formula weight of CNT in the calculation.

4.3 *In Situ* Bismuth Film on CNT Modified Glassy Carbon (*In Situ* BiF/CNT/GC) Electrode

4.3.1 Electrochemical Characterization of CNT Modified Glassy Carbon (CNT/GC) Electrode

Background current for the CNT/GC electrode was obtained by means of cyclic voltammetry. Fig. 4.6 shows cyclic voltammograms of the bare GC electrode and the CNT/GC electrode in 0.1 M acetate buffer solution (pH 4.5) scanned from 1.00 to –1.50 V and –1.50 to 1.00 V at the sweep rate of 100 $mV \cdot s^{-1}$. It

can be seen that the CNT/GC electrode exhibited higher background current than the bare GC electrode, implying that the modified CNTs, can change the electrical properties of the GC substrate. This observation was similar to the result from previous work, which described that CNTs produced relatively high background current, arising mainly from double layer charging proportional to the electrode surface area [10]. Note that all potentials are quoted with silver/silver chloride (Ag/AgCl) reference electrode which has the potential value of 0.22 V *versus* standard hydrogen electrode (SHE).

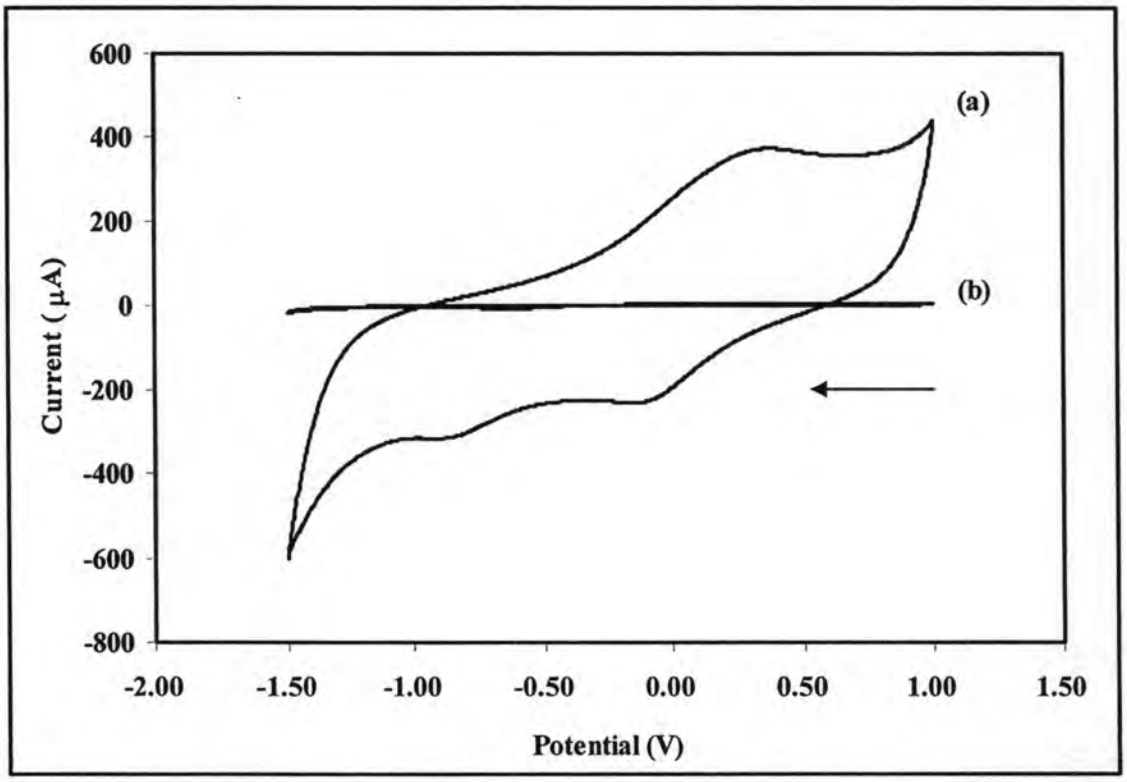

Figure 4.6 Cyclic voltammograms for 0.1 M acetate buffer solution (pH 4.5) recorded with (a) CNT/GC electrode and (b) bare GC electrode at the scan rate of 100 $mV \cdot s^{-1}$.

4.3.2 Electrochemical Responses of *In Situ* Bismuth Film on CNT Modified Glassy Carbon (*In Situ* BiF/CNT/GC), *In Situ* Bismuth Film on Glassy Carbon (*In Situ* BiF/GC), CNT Modified Glassy Carbon (CNT/GC), and Glassy Carbon (GC) Electrodes towards Cadmium (II) and Lead (II) Ions

To understand the effects of bismuth film towards the determination of cadmium (II) and lead (II) ions by square wave anodic stripping voltammetry

(SWASV), the stripping voltammograms for 25 $\mu g \cdot L^{-1}$ of both metal ions recorded with *in situ* BiF/CNT/GC electrode (Fig. 4.7a), *in situ* BiF/GC electrode (Fig. 4.7b), CNT electrode (Fig. 4.7c), and bare GC electrode (Fig. 4.7d) were employed. For the cases of *in situ* bismuth film electrodes (Fig. 4.7a-4.7b), the solution of bismuth (III) ions was added to the metal ion solution for the preparation of bismuth film. During the deposition, the formation of bismuth film and its alloys with cadmium and lead, Cd(Bi) and Pb(Bi), were generated as equations 4.1 and 4.2.

$$Bi^{3+}(aq) + 3e^{-} \rightleftharpoons Bi\,(s) \qquad (4.1)$$

$$M^{2+}(aq) + 2e^{-} + Bi\,(s) \rightleftharpoons M(Bi)\,(s) \qquad (4.2)$$

When M represents cadmium or lead metal, while M^{2+} depicts cadmium (II) or lead (II) ion. In the stripping step, Cd(Bi) and (Pb)Bi alloys were oxidized to yield the cadmium (II), lead (II), and bismuth (III) ion stripping peaks appearing at about the potentials of –0.86, –0.63, and –0.23 V, respectively. In terms of electrode sensitivity, the *in situ* BiF/CNT/GC electrode exhibited the highest stripping responses towards cadmium (II) and lead (II) ions, followed by the *in situ* BiF/GC electrode. These results have revealed that CNTs are better film support than the bare GC. Similar results had been observed by Hwang and co-workers, who demonstrated that the sensitivity of the *in situ* bismuth film on CNT electrode was two times higher than that of GC electrode [10]. On the contrary, without the bismuth film, only the tiny peak of cadmium (II) ions was observed at the bare CNT/GC electrode and no peaks corresponding to these two metal ions were found at GC electrode, implying the significance of bismuth film for stripping analysis of the target metal ions. These findings about the necessity of bismuth film are in agreement with the results in earlier literatures [8,22]. The broad peak at potential more positive than –0.20 V found in Fig. 4.7a and 4.7c represented the characteristic of CNT electrode. In conclusion, the synergistic effect of bismuth film and CNT electrode makes *in situ* BiF/CNT/GC electrode be appropriate electrode for probing cadmium (II) and lead (II) ions.

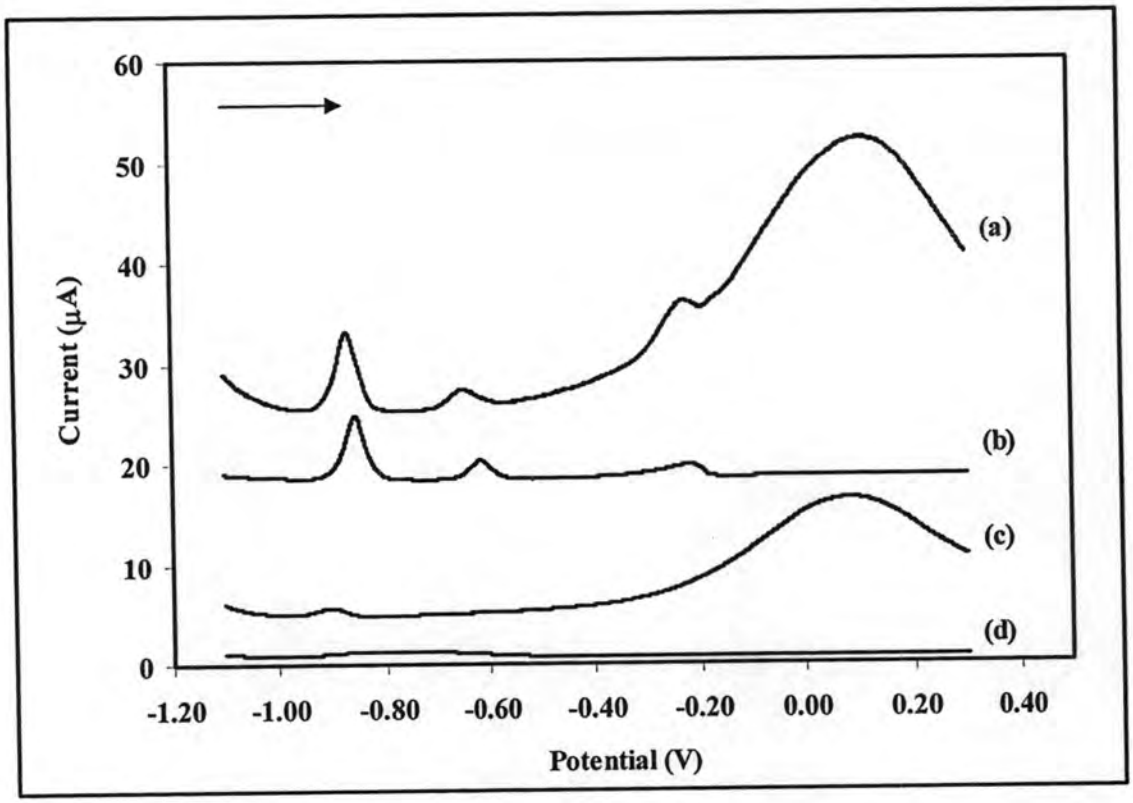

Figure 4.7 SWASV voltammograms for 0.1 M acetate buffer solution (pH 4.5) containing 25 $\mu g \cdot L^{-1}$ of cadmium (II) and lead (II) ions recorded with (a) *in situ* BiF/CNT/GC electrode, (b) *in situ* BiF/GC electrode, (c) CNT/GC electrode, and (d) GC electrode with the deposition potential of –1.10 V, the deposition time of 120 s, and the scan rate of 7.5 $mV \cdot s^{-1}$.

4.3.3 Optimization of Experimental Parameters for The Determination of Cadmium (II) and Lead (II) Ions by *In Situ* Bismuth Film on CNT Modified Glassy Carbon (*In Situ* BiF/CNT/GC) Electrode

To obtain better electrochemical performance from the *in situ* BiF/CNT/GC electrode, the experimental conditions (*e.g.*, the presence of dioxygen (O_2), the quantity of Nafion on bismuth film, and the concentration of bismuth (III) ion precursor) were optimized.

4.3.3.1 Effect of Dioxygen (O_2)

O_2 is known to be an interference for the trace determination of heavy metal ions by typical mercury electrodes, but previous work has revealed that

the bismuth electrodes are insensitive to the presence of O_2 [41]. In order to confirm the O_2 insensitivity of bismuth electrodes, SWASV analyses of cadmium (II) and lead (II) ions in the absence and presence of O_2 were compared. Fig. 4.7 shows the effect of O_2 on the cadmium (II) and lead (II) ion stripping peaks at *in situ* BiF/CNT/GC electrodes. In both cases, the peak potentials and heights of each metal ion are similar. This figure shows that bismuth electrodes can be conveniently performed in the undeoxygenated condition.

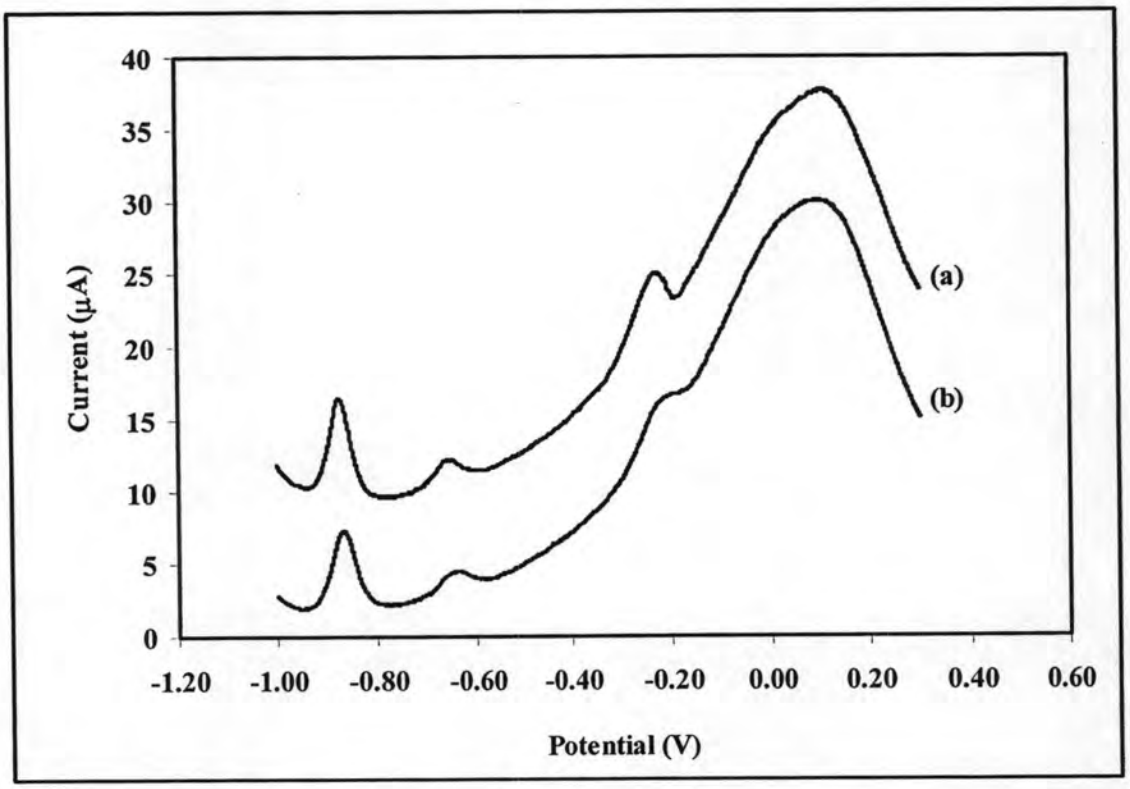

Figure 4.8 SWASV voltammograms for 0.1 M acetate buffer solution (pH 4.5) containing 25 $\mu g \cdot L^{-1}$ of cadmium (II) and lead (II) ions recorded with *in situ* BiF/CNT/GC electrodes in the (a) presence and (b) absence of O_2 using the deposition potential of –1.10 V, the deposition time of 120 s, and the scan rate of 7.5 $mV \cdot s^{-1}$.

4.3.3.2 Effect of Nafion

Nafion, a perfluorosulfonated and negatively charged polymer, was used to improve the sensitivity of *in situ* BiF/CNT/GC electrode for the determination of cadmium (II) and lead (II) ions. Xu and co-workers have found that permselective Nafion film on the bismuth film electrode can significantly improve the

sensitivity, surfactant tolerance, and long-term stability of the electrode [22]. Thus, Fig. 4.9 exhibits the effect of Nafion towards the stripping currents for cadmium (II) and lead (II) ions, displaying that the best stripping signals for both metal ions were obtained by *in situ* BiF/CNT/GC electrodes prepared with 0.50% Nafion. Therefore, the 0.50% Nafion was then used for the preparation of *in situ* BiF/CNT/GC electrodes. However, the lower stripping currents at 0.75% and 1.00% Nafion revealed that it might be unfavorable to electrodeposit metal ions onto the electrode with thick Nafion film.

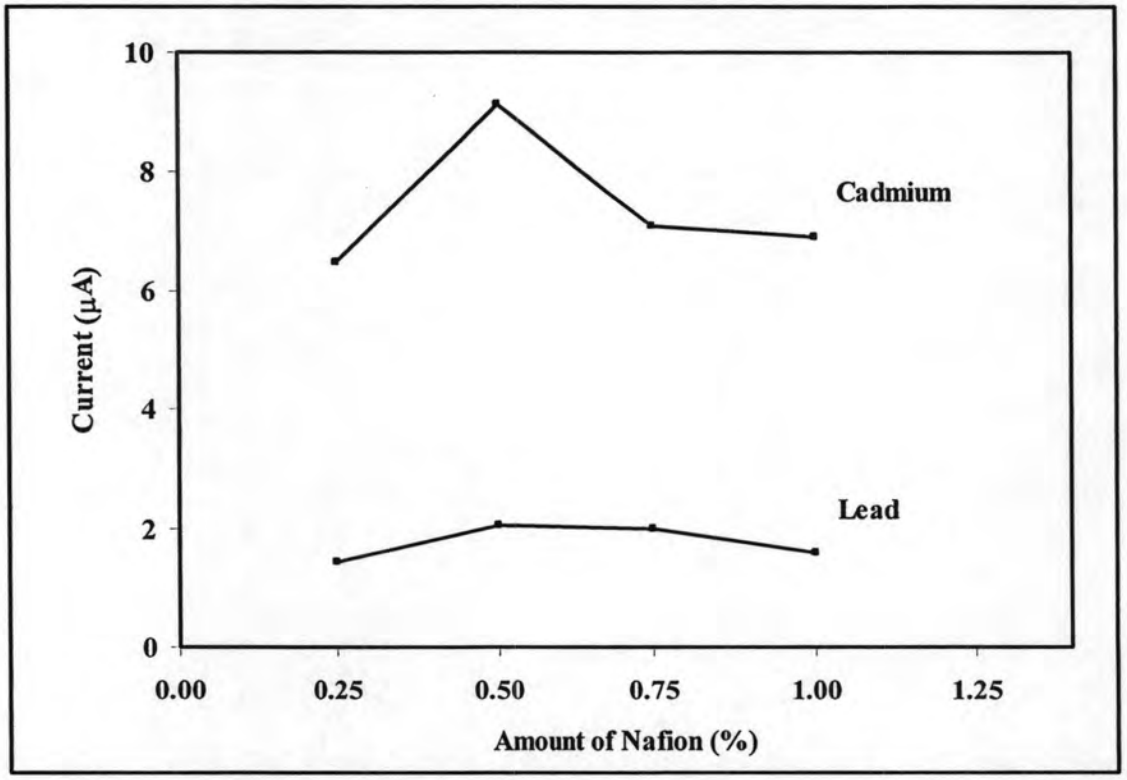

Figure 4.9 Effect of Nafion amount on the stripping peak currents for 25 $\mu g \cdot L^{-1}$ of cadmium (II) and lead (II) ions in 0.1 M acetate buffer solutions (pH 4.5) recorded with *in situ* BiF/CNT/GC electrodes by SWASV using the deposition potential of –1.10 V, the deposition time of 120 s, and the scan rate of 7.5 $mV \cdot s^{-1}$.

4.3.3.3 Effect of Bismuth (III) Ion Concentration

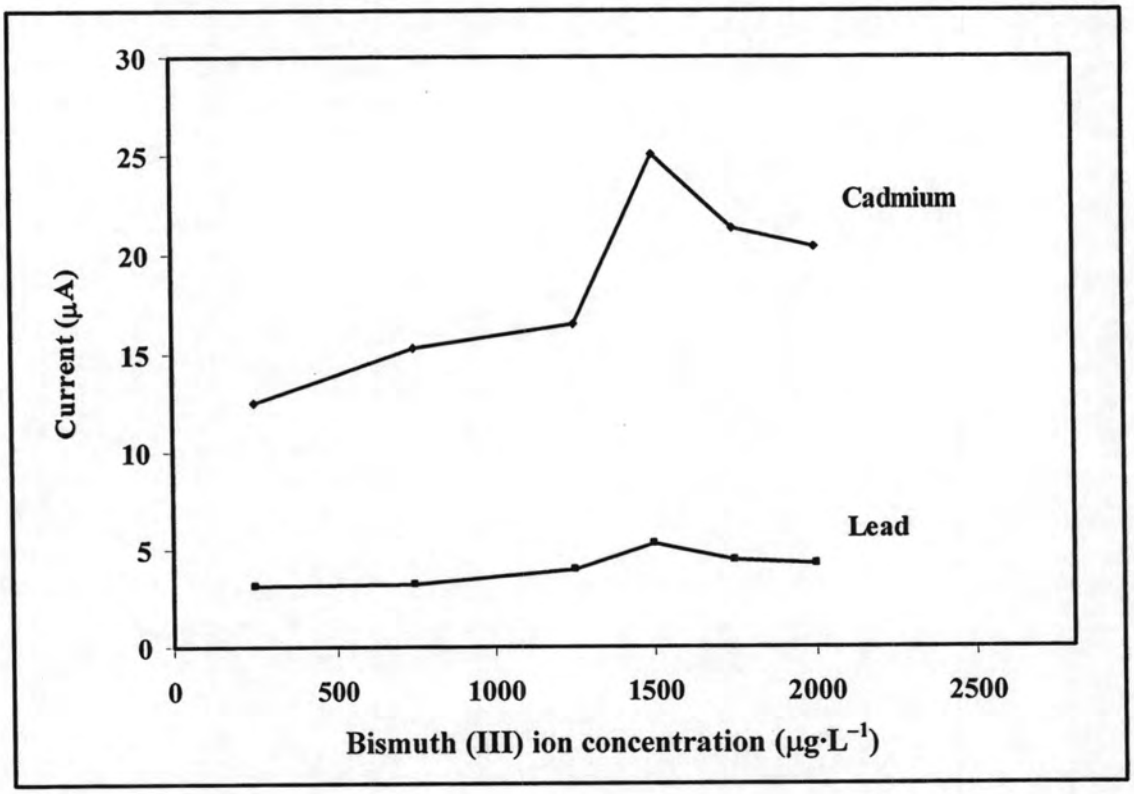

(a)

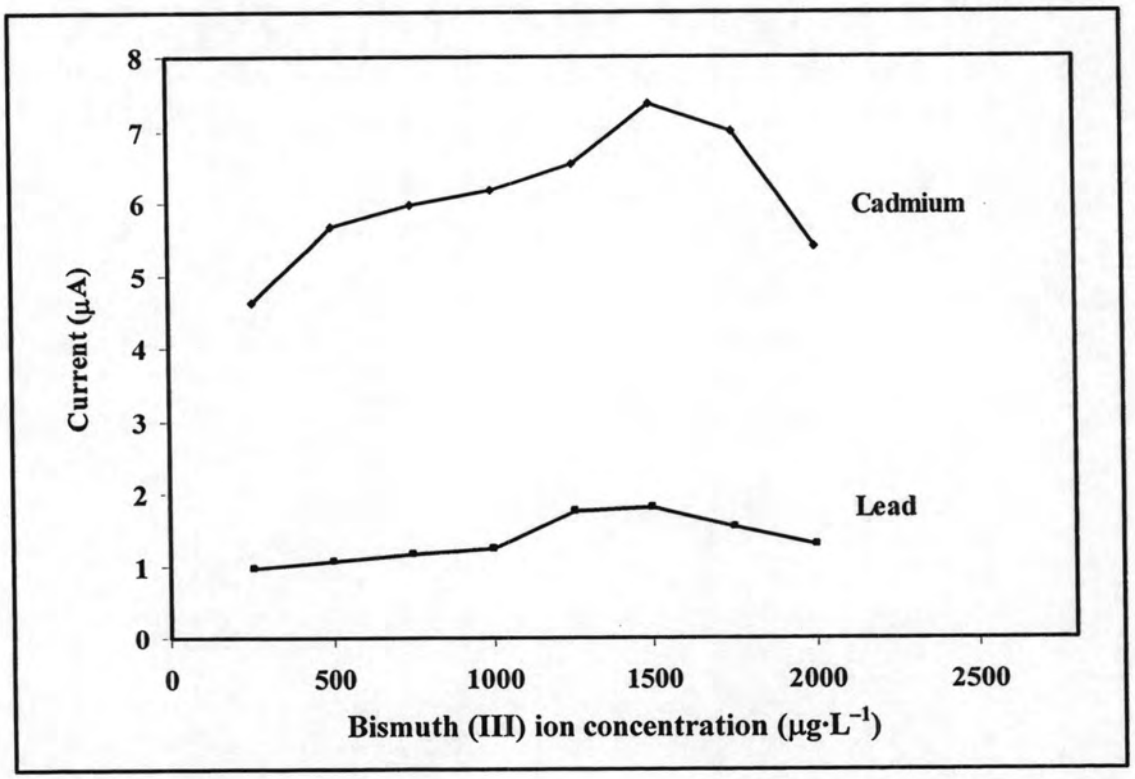

(b)

Figure 4.10 Effect of bismuth (III) ion concentration on the stripping peak currents for (a) 25 $\mu g \cdot L^{-1}$ and (b) 80 $\mu g \cdot L^{-1}$ of cadmium (II) and lead (II) ions in 0.1 M acetate

buffer solutions (pH 4.5) recorded with *in situ* BiF/CNT/GC electrodes by SWASV using the same experimental conditions as those in Fig. 4.9.

For SWASV analysis by *in situ* BiF/CNT/GC electrodes, the influence of bismuth (III)-ion precursor concentration on the stripping peak currents of cadmium (II) and lead (II) ions are shown in Fig. 4.10. The effect of bismuth (III) ions was investigated in the concentration range of 250 to 2,000 $\mu g \cdot L^{-1}$ for the solutions containing (a) 25 $\mu g \cdot L^{-1}$ and (b) 80 $\mu g \cdot L^{-1}$ of cadmium (II) and lead (II) ions in order to compare the results at different metal-ion concentrations. Similar to the observation in previous work [22], the concentration of bismuth (III) ions controlls the thickness of the bismuth film, but it does not affect the peak positions of both heavy metal ions. According to Fig. 4.10, the bismuth (III) ion concentration of 1,500 $\mu g \cdot L^{-1}$ was used for subsequent analytical work by the *in situ* bismuth film electrodes since this bismuth concentration provided the highest peak currents for both heavy metal ions at different concentration ranges.

4.3.3.4 Effect of Deposition Potential

Various researches have studied the effect of the deposition potential on the stripping signals of metal ions with bismuth electrodes and reported that the sensitivity of the bismuth electrode depends on the deposition potential at preconcentration step. Thus, the plots of the stripping responses of cadmium (II) and lead (II) ions *versus* the deposition potential is shown in Fig. 4.11. The deposition potential for SWASV was investigated in the range from –0.95 to –1.30 V. As the deposition potential became more negative, the peak currents of both heavy metal ions increased to gain the highest values at the deposition potential of –1.10 V. This increasing trend of the stripping currents with the deposition potential arose from the fact that there were more Cd(Bi) and Pb(Bi) alloy formed at more negative potential. However, the stripping currents of both metal ions significantly decreased their sizes after the deposition potential shifted negatively from –1.10 V, implying that either these deposition conditions might not be appropriate for the formation of bismuth alloys or there might be other on-going processes competing with the alloy formation. Therefore, the potential of –1.10 V was thus chosen as the deposition potential for SWASV analysis.

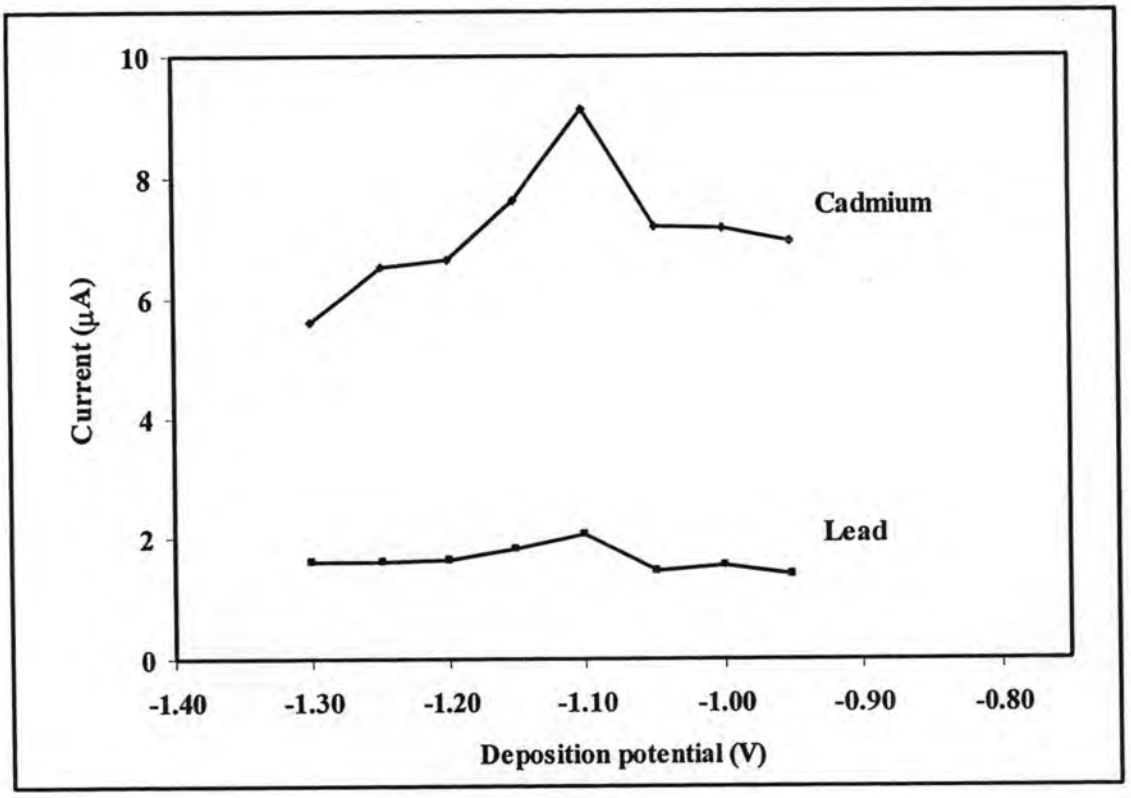

Figure 4.11 Effect of the deposition potential on the stripping peak currents for 25 $\mu g \cdot L^{-1}$ of cadmium (II) and lead (II) ions in 0.1 M acetate buffer solutions (pH 4.5) recorded with *in situ* BiF/CNT/GC electrodes by SWASV using the same experimental conditions as those in Fig. 4.9.

4.3.3.5 Effect of Deposition Time

The deposition time for the stripping analysis of cadmium (II) and lead (II) ions by *in situ* BiF/CNT/GC electrode was varied from 30 s to 900 s and its effect towards the stripping currents is demonstrated in Fig. 4.12. For lead (II) ion, the peak current increased proportionally with the deposition time. For cadmium (II) ion, the stripping peak also enhanced directly with the deposition time; however, the increment slightly dropped at higher deposition times ranging from 540 to 900 s. The decrease in the electrode sensitivity could be explained by the hypothesis that thicker bismuth film arisen from longer deposition might contain more bismuth self-agglomerate that can possibly interfere the formation of bismuth alloys. Therefore, the deposition time of 30 to 540 s could be effectively used, but the 120-s deposition time was selected in this work to obtain rapid and efficient analysis. Similar results had been observed by Torma and co-workers, who reported that the stripping

responses at the Nafion/2,2′-bipyridyl/bismuth composite film electrode increased linearity with increasing the deposition time [23].

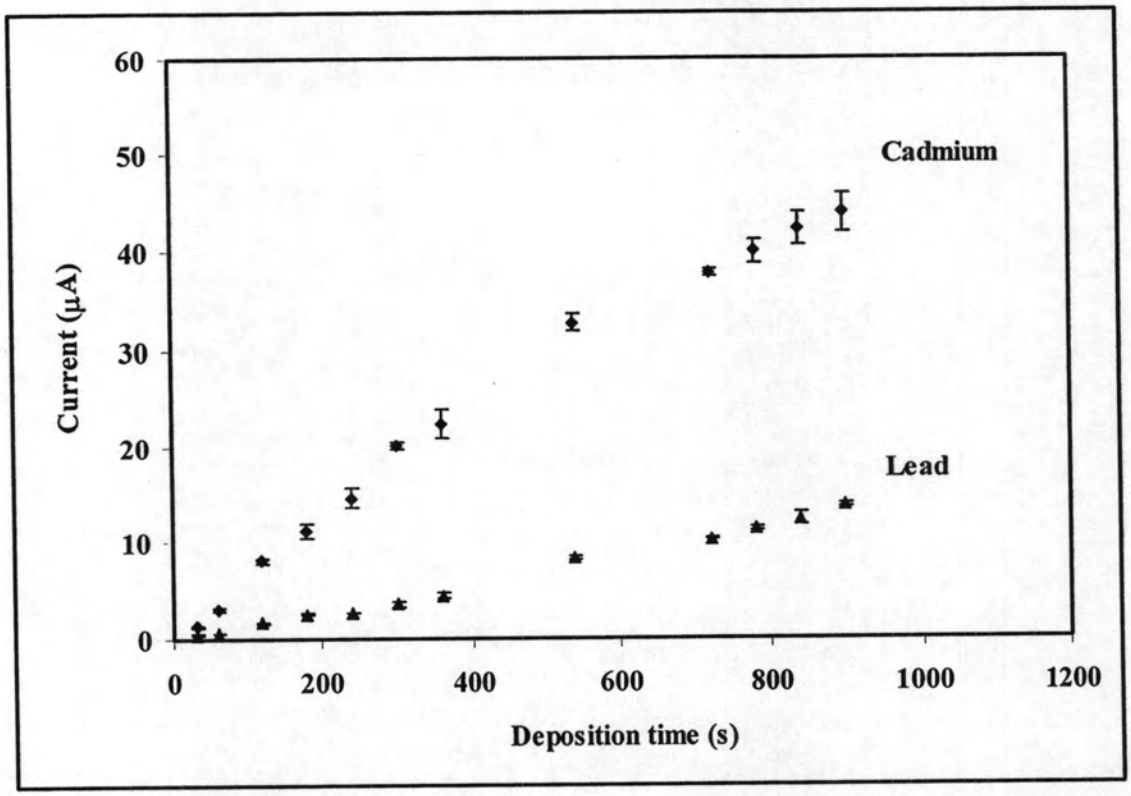

Figure 4.12 Effect of the deposition time on the stripping peak currents for 25 $\mu g \cdot L^{-1}$ of cadmium (II) and lead (II) ions in 0.1 M acetate buffer solutions (pH 4.5) recorded with *in situ* BiF/CNT/GC electrodes by SWASV using the same experimental conditions as those in Fig. 4.9.

4.3.4 Calibration Curves of *In Situ* Bismuth Film on CNT Modified Glassy Carbon (*In Situ* BiF/CNT/GC) Electrode

Simultaneous determination of lead (II) and cadmium (II) ions with *in situ* BiF/CNT/GC electrodes was performed and the calibration curves are displayed in Fig. 4.13. These curves present the stripping peak currents obtained from *in situ* BiF/CNT/GC electrodes (y-axis) for the determination of 5-80 $\mu g \cdot L^{-1}$ metal ion concentration (x-axis). In the calibration curves, the plotted values are the average values of three repetitive measurements. The curves show excellent linearity with correlations (R^2) of 0.9987 for cadmium (II) ion (Fig. 4.13a) and 0.9978 for lead (II) ion (Fig. 4.13b). The peak currents increased linearly with metal ion concentration, with slopes of 0.142 $\mu A\ L \cdot \mu g^{-1}$ for cadmium (II) ion and $4.18 \times 10^{-2}\ \mu A\ L \cdot \mu g^{-1}$ for lead (II) ion. These results have suggested that the *in situ* BiF/CNT/GC electrode is more sensitive towards cadmium (II) ion than lead (II) ion. Determined as the concentration corresponding to a current three times the average background current, the limits of detection (LODs) were 2.0 $\mu g \cdot L^{-1}$ for both cadmium (II) and lead (II) ions. In comparison with the previously reported bismuth film electrode [32], the detection limit values for cadmium (II) and lead (II) ions were lower. Defined as the lowest concentration of the calibration curve, the limits of quantification (LOQs) [55] were 5.0 $\mu g \cdot L^{-1}$ for these two heavy metal ions. Moreover, the reproducibility of *in situ* BiF/CNT/GC electrode was indicated by the relative standard deviations of 6.91% for cadmium (II) ion and 9.86% for lead (II) ion at the 25 $\mu g \cdot L^{-1}$ concentration level (n = 8).

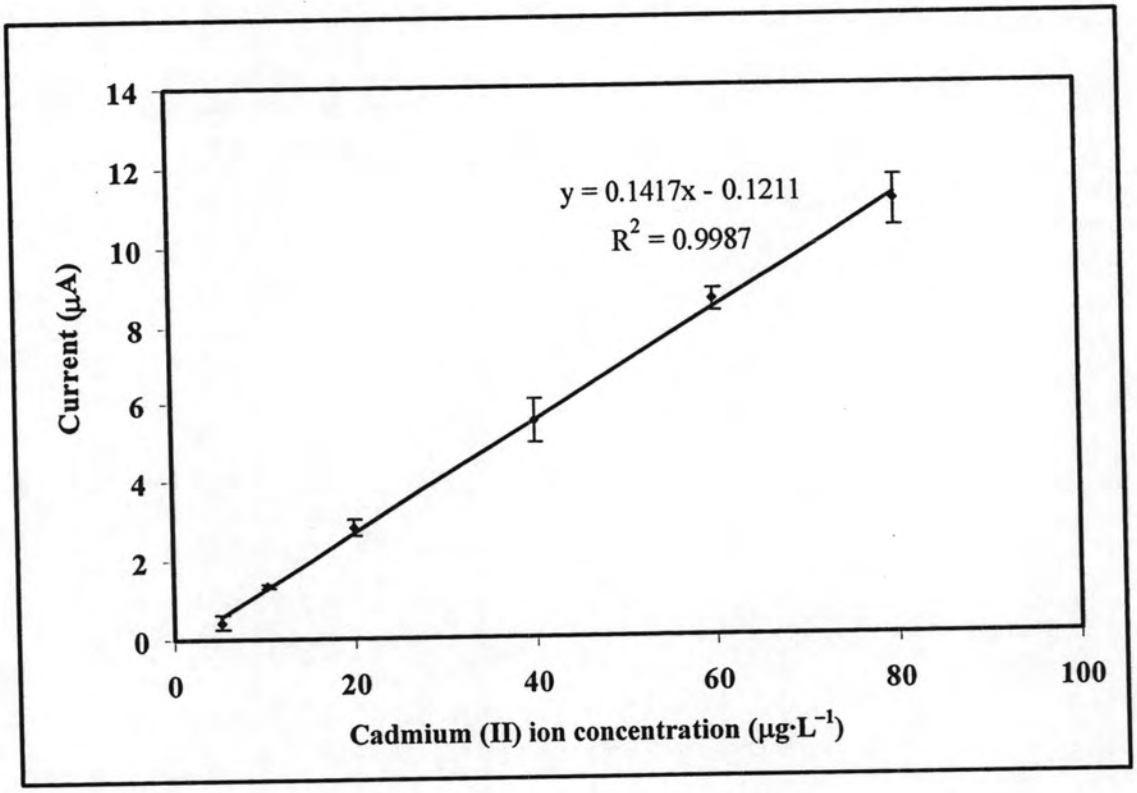

(a)

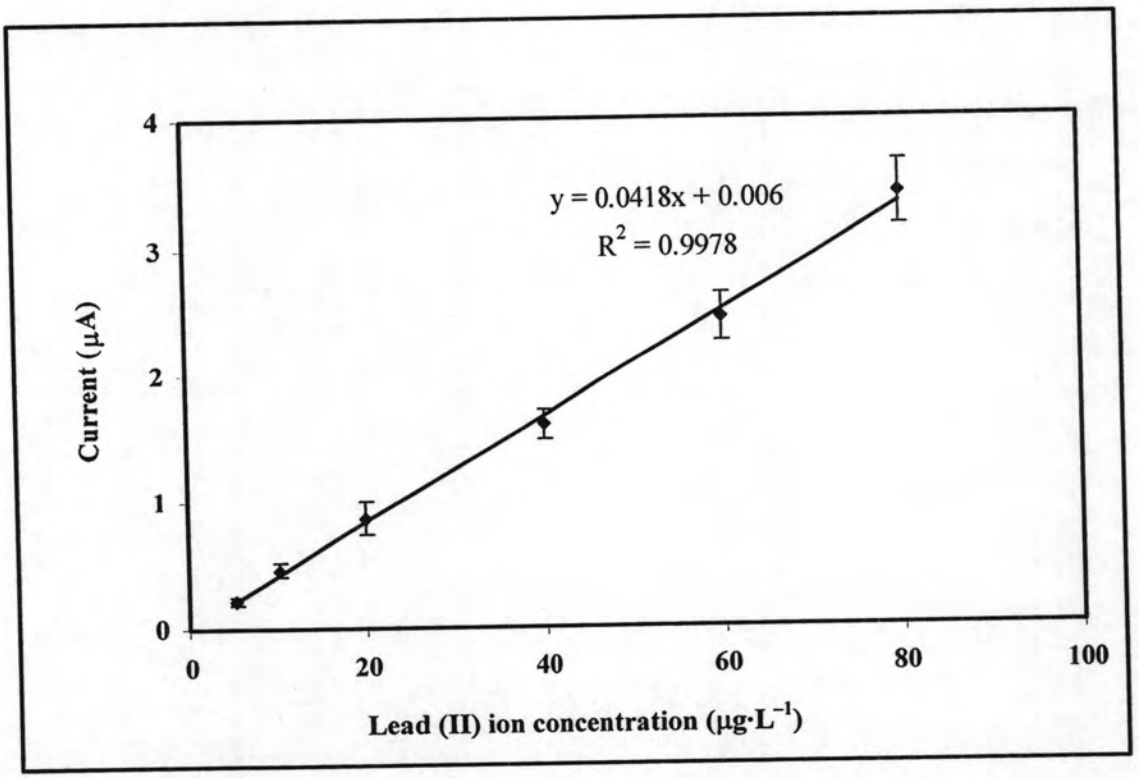

(b)

Figure 4.13 Calibration plots of (a) cadmium (II) and (b) lead (II) ions from SWASV analysis by *in situ* BiF/CNT/GC electrodes in 0.1 M acetate buffer solutions using the same experimental conditions as those in Fig. 4.9.

4.4 Bi–CNT Composite Modified Glassy Carbon (Bi–CNT/GC) Electrode

According to the observation in Section 4.3, it can be possibly concluded that *in situ* BiF/CNT/GC electrodes have interesting features for the analysis of cadmium (II) and lead (II) ions. Nevertheless, the inconvenience for the preparation of bismuth film has drawn the attention to the new Bi–CNT composite modified electrodes.

4.4.1 Electrochemical Characterization of Bi–CNT Composite Modified Glassy Carbon (Bi–CNT/GC) Electrode

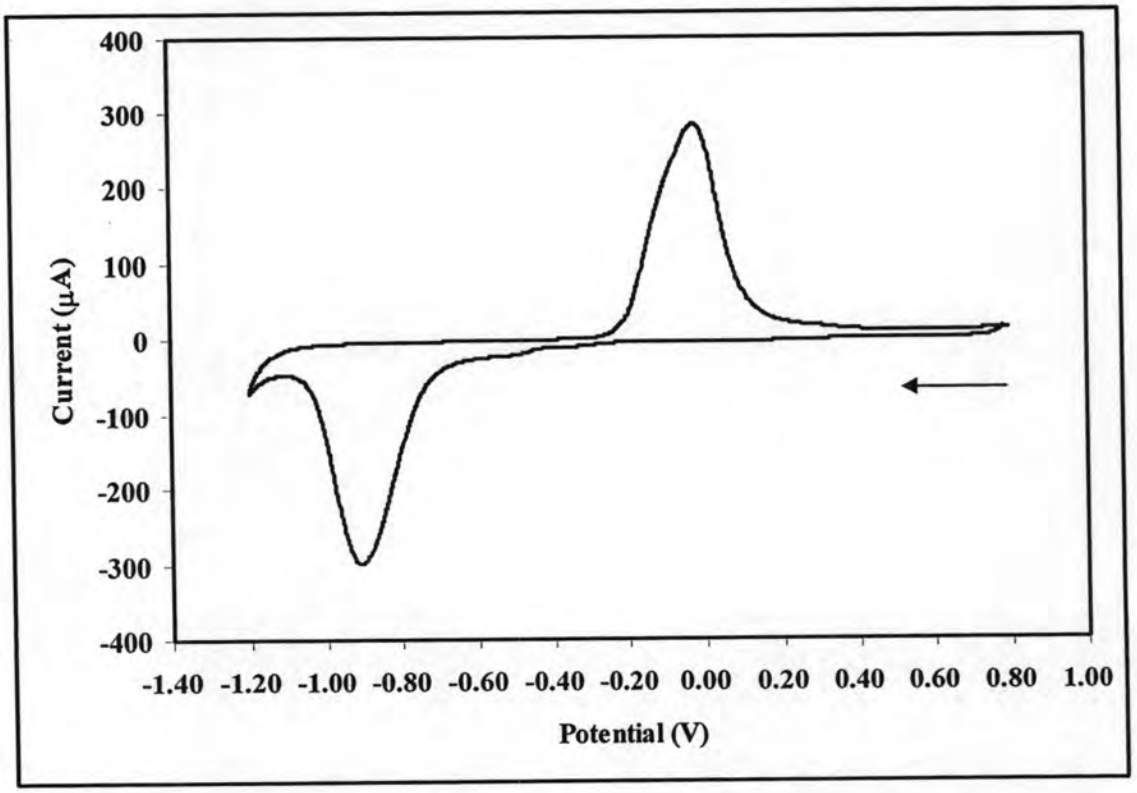

Figure 4.14 Cyclic voltammogram for 0.1 M acetate buffer solution (pH 4.5) recorded with 4.00 mol % Bi–CNT/GC electrode at the scan rate of 100 $mV \cdot s^{-1}$.

Fig. 4.14 displays cyclic voltammogram of the GC electrode modified with 4.00 mol % Bi–CNT composite scanned in 0.1 M acetate buffer solution (pH 4.5) from +0.80 to –1.20 V and –1.20 to +0.80 V at the scan rate of 100 $mV \cdot s^{-1}$. The cathodic and anodic peaks of bismuth (III)–bismuth (0) redox couple [41] were observed with the peak potentials of –0.89 and –0.08 V, respectively. This voltammogram not only confirmed that bismuth was successfully deposited on the

surface of CNTs by this selected method, but revealed that the GC electrode modified with Bi–CNT composite could be successfully fabricated.

4.4.2 Comparison between Bi–CNT Composite Modified Glassy Carbon (Bi–CNT/GC) Electrode and *In Situ* Bismuth Film on CNT Modified Glassy Carbon (*In Situ* BiF/CNT/GC) Electrode towards The Determination of Cadmium (II) and Lead (II) Ions

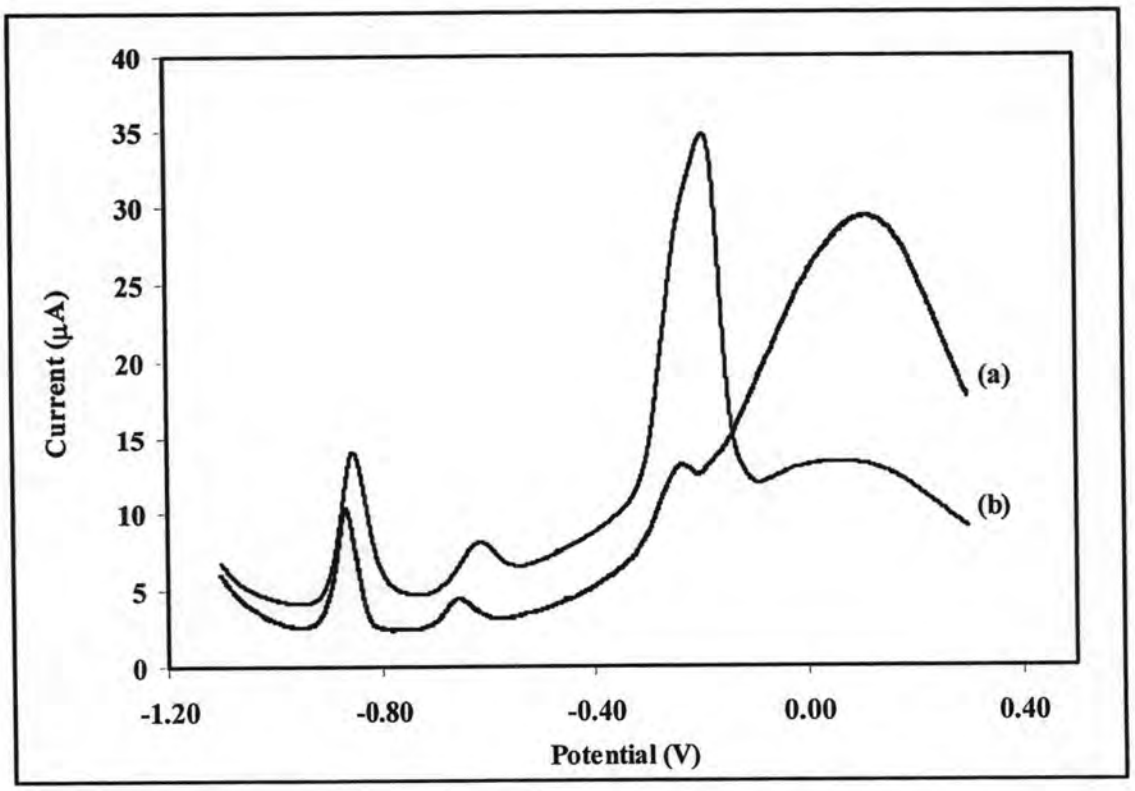

Figure 4.15 SWASV signals obtained from (a) *in situ* BiF/CNT/GC electrode and (b) 2.00 mol % Bi–CNT/GC electrode for 0.1 M acetate buffer solution (pH 4.5) containing 25 $\mu g \cdot L^{-1}$ of cadmium (II) and lead (II) ions with the deposition potential of –1.10 V, the deposition time of 120 s, and the scan rate of 7.5 $mV \cdot s^{-1}$.

Stripping voltammograms for 25 $\mu g \cdot L^{-1}$ of cadmium (II) and lead (II) ions obtained at two types of bismuth electrodes are illustrated in Fig. 4.15. For both *in situ* BiF/CNT/GC and Bi–CNT/GC electrodes, the potentials for the stripping peaks of cadmium (II) and lead (II) ions were approximately the same. With 120-s deposition at the potential of –1.10 V, well-defined and sharp stripping peaks were observed at both bismuth electrodes. For cadmium (II) ion showing the stripping

peak at about –0.86 V, the peak currents of 7.80 μA and 10.19 μA were obtained from *in situ* BiF/CNT/GC electrode and Bi–CNT/GC electrode, respectively. For the stripping peak currents of lead (II) ion at the potential of –0.62 V, the bismuth film modified electrode gave 1.67 μA whereas the Bi–CNT modified electrode led to 1.94 μA. This comparison undoubtedly demonstrated that the Bi–CNT modified electrode can remarkably improve the sensitivity for the determination of these heavy metal ions compared to *in situ* BiF/CNT/GC electrode. Note that the peaks at approximately –0.23 V observed at both bismuth modified electrodes show the oxidation of bismuth film to bismuth (III) ion.

4.4.3 Optimization of Experimental Parameters for The Determination of Cadmium (II) and Lead (II) Ions by Bi–CNT Composite Modified Glassy Carbon (Bi–CNT/GC) Electrode

Similar to the case of *in situ* BiF/CNT/GC electrode, experimental parameters for the determination of cadmium (II) and lead (II) ions were carefully optimized.

4.4.3.1 Effect of Nafion

Fig. 4.16 describes the variation in the SWASV peak currents for cadmium (II) and lead (II) ions as a function of Nafion amount added during the electrode preparation. The stripping peak currents of both metal ions increased dramatically with the amount of Nafion from 0.25 to 0.50% and maintained their values, especially those of lead (II) ion, with 0.50 to 0.75% Nafion. When the Nafion quantity was higher than 0.75%, the decrease in the peak currents for both metal ions was observed. In order to achieve direct comparison with the results from *in situ* BiF/CNT/GC electrodes using 0.50% Nafion for their preparation, the 0.50% Nafion that provided the stripping current heights approximately the same or near the highest values (at 0.75% Nafion) was chosen for the preparation of all Bi–CNT modified electrodes reported in this thesis.

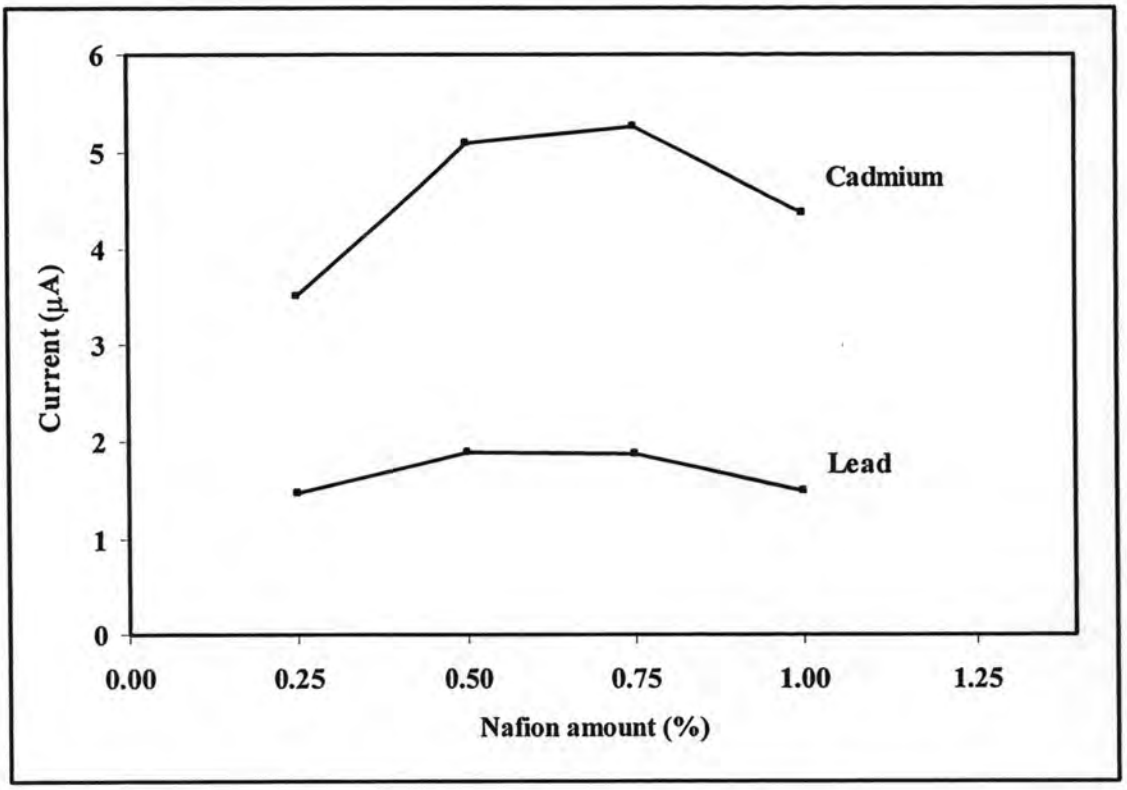

Figure 4.16 Effect of Nafion amount on the stripping currents for 25 $\mu g \cdot L^{-1}$ of cadmium (II) and lead (II) ions in 0.1 M acetate buffer solutions (pH 4.5) recorded with Bi–CNT/GC electrodes by SWASV using the same experimental conditions as those in Fig. 4.15.

4.4.3.2 Quantity of Bismuth in Bi–CNT Composite

In Fig. 4.17, the effect of bismuth quantity in Bi–CNT composite on the SWASV responses of a Bi–CNT/GC electrode analyzed in a solution containing 25 $\mu g \cdot L^{-1}$ cadmium (II) and lead (II) ions is displayed. As bismuth content in the modified electrode was increased up to 2.00 mol %, the stripping responses enhanced due to more active sites of the bismuth in the electrode. However, the sensitivity of the Bi–CNT/GC electrode towards metal ion determination decreased dramatically when more than 2.00 mol % of bismuth in the composite was used. Hence, the Bi–CNT modified electrodes containing 2.00 mol % of bismuth in Bi–CNT composite were used for subsequent metal ion measurements. Additionally, it is important to point out that the mol % of bismuth discussed in this section was actually calculated from the bismuth precursor used in the synthesis of composite.

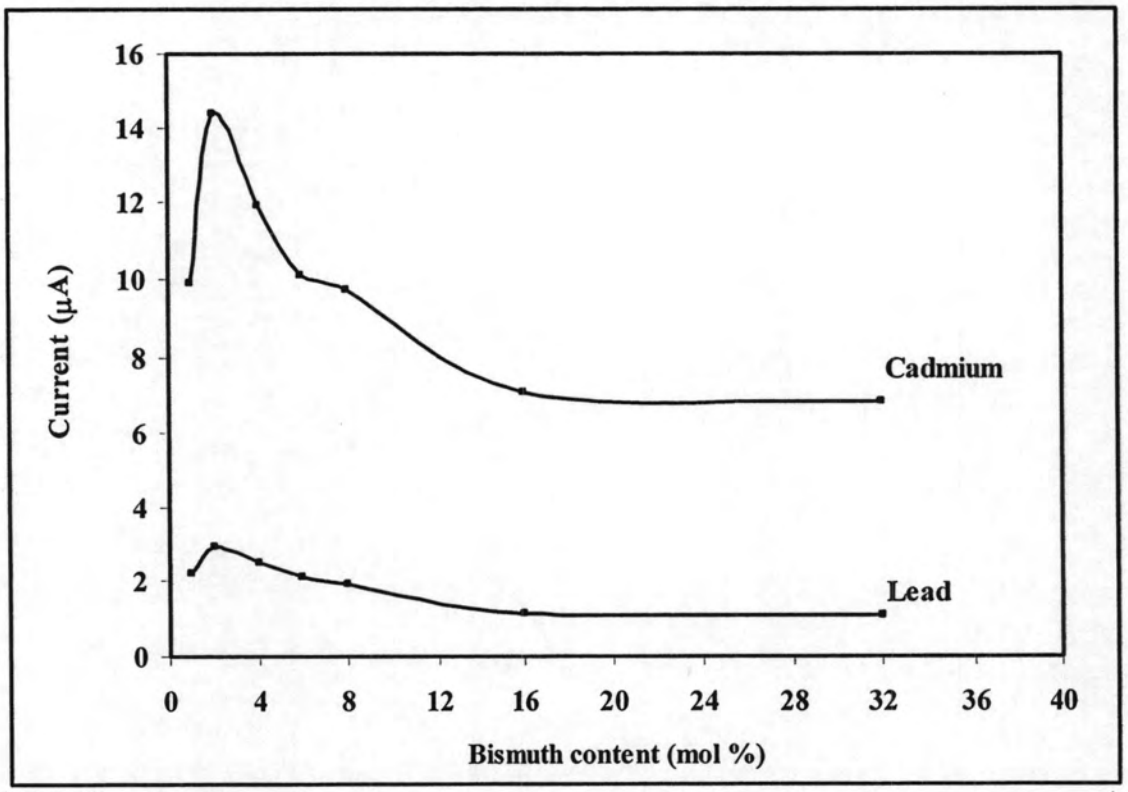

Figure 4.17 Effect of bismuth content in Bi–CNT composite on the stripping voltammetric responses for 25 $\mu g \cdot L^{-1}$ of cadmium (II) and lead (II) ions in 0.1 M acetate buffer solutions (pH 4.5) recorded with Bi–CNT/GC electrodes by SWASV using the same experimental conditions as those in Fig. 4.15.

4.4.3.3 Effect of Deposition Potential

Since deposition potential is an important parameter in stripping analysis that influences the sensitivity for the determination, the effect of the deposition potential on the stripping signals for cadmium (II) and lead (II) ions was studied in the potential range from –1.00 to –1.20 V (Fig. 4.18). As the potential shifted negatively from –1.00 to –1.10 V, the stripping currents for cadmium (II) and lead (II) ions increased. At the deposition potentials more negative than –1.10 V, the peak current heights were lower than the values obtained at the deposition potential of –1.10 V. Therefore, the deposition potential of –1.10 V was selected for further work.

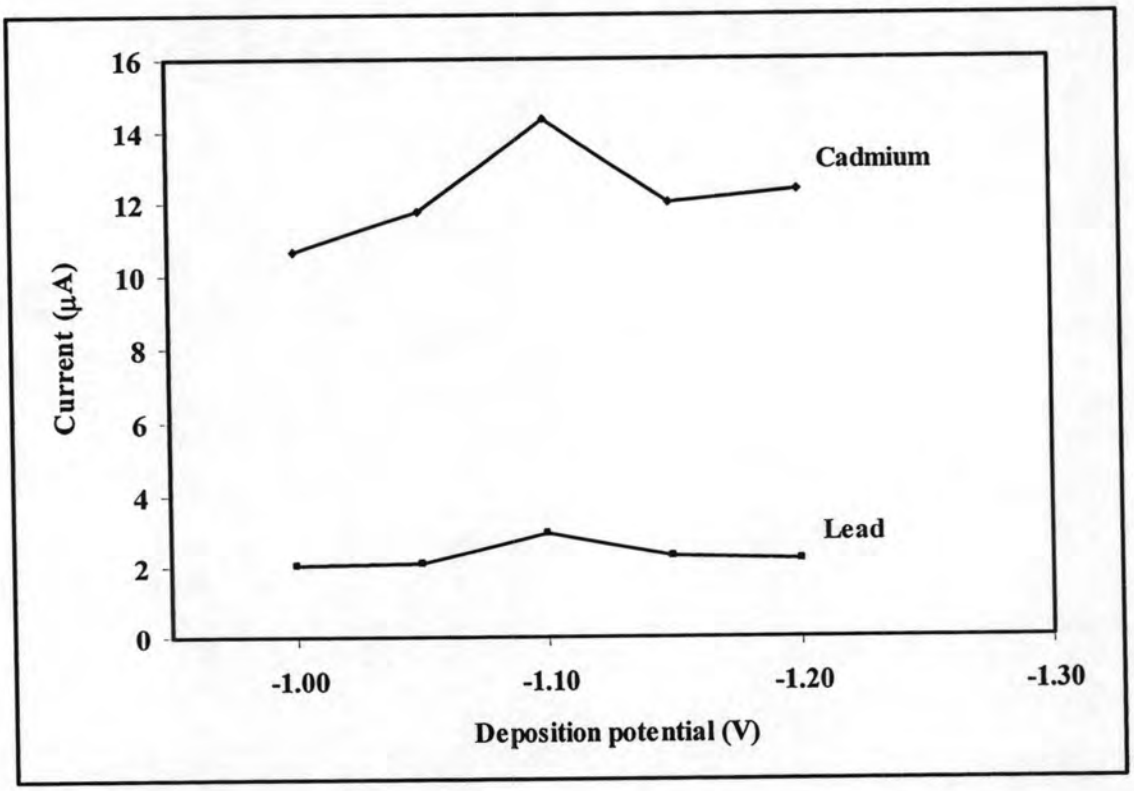

Figure 4.18 Effect of the deposition potential on the stripping peak currents for 25 $\mu g \cdot L^{-1}$ of cadmium (II) and lead (II) ions in 0.1 M acetate buffer solutions (pH 4.5) recorded with 2.00 mol % Bi–CNT/GC electrodes by SWASV using the same experimental conditions as those in Fig. 4.15.

4.4.3.4 Effect of Deposition Time

As seen in Fig. 4.19, the effect of deposition time on the SWASV peak currents of cadmium (II) and lead (II) ions were tested. The deposition time was varied from 30 to 900 s using the electrode modified by Bi–CNT composite with 2.00 mol % of bismuth. The peak currents for both heavy metal ions increased proportionally with the deposition time. Thus, the whole range of 30 to 900 s could be effectively used as the deposition time in SWASV analysis; however, 120-s deposition time was selected in this work to obtain rapid and efficient analysis as well as direct comparison with the *in situ* BiF/CNT/GC electrode result.

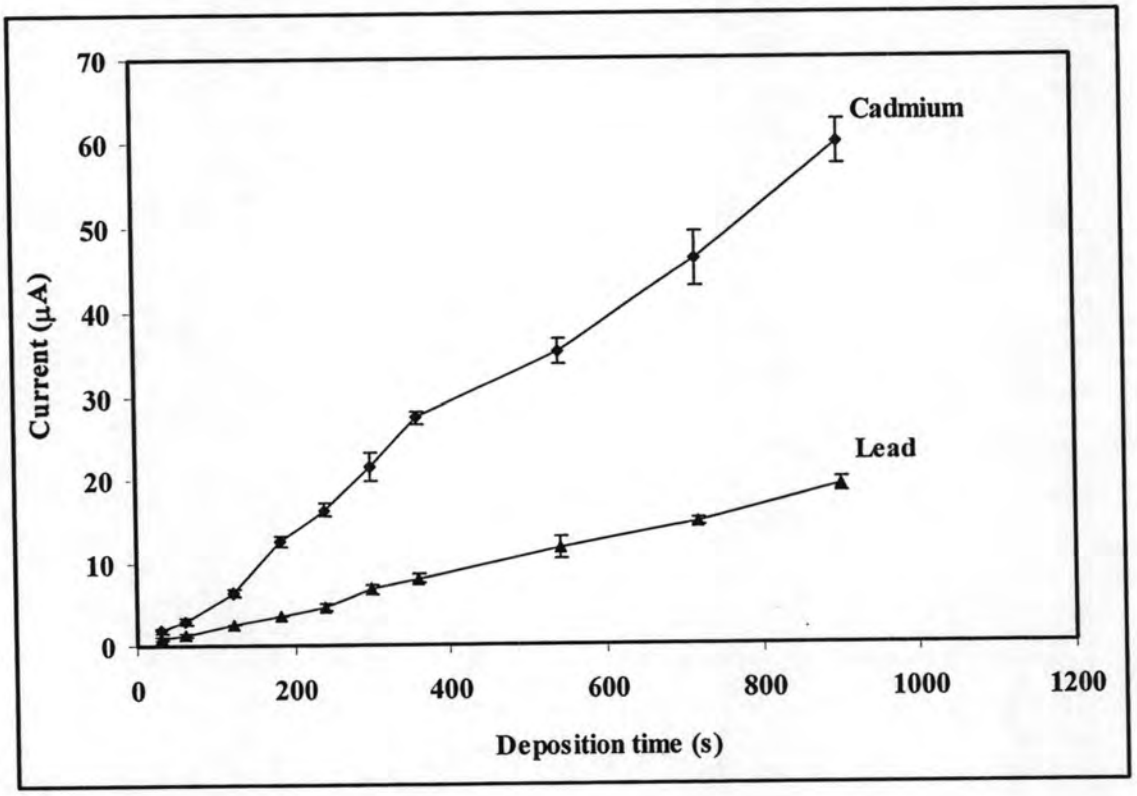

Figure 4.19 Effect of the deposition time on the stripping peak currents for 25 $\mu g \cdot L^{-1}$ of cadmium (II) and lead (II) ions in 0.1 M acetate buffer solutions (pH 4.5) recorded with 2.00 mol % Bi–CNT/GC electrodes by SWASV using the same experimental conditions as those in Fig. 4.15.

4.4.4 Calibration Curves of Bi–CNT Composite Modified Glassy Carbon (Bi–CNT/GC) Electrode

After optimizing various experimental parameters, the calibration plots of cadmium (II) and lead (II) ions obtained from SWASV analysis by 2.00 mol % Bi–CNT/GC electrodes were investigated. Fig. 4.20 shows the calibration curves of cadmium (II) and lead (II) ions, which were found to contain two linear ranges. The first range of calibration curve is at the concentrations between 5 to 150 $\mu g \cdot L^{-1}$ and the R^2 values for cadmium (II) and lead (II) ions are 0.9986 and R^2 = 0.9990, respectively. For the second range, the calibration curves of cadmium (II) ion (R^2 = 0.9983) and lead (II) ion (R^2 = 0.9970) are from 150 to 240 $\mu g \cdot L^{-1}$. For cadmium (II) and lead (II) ions, the LODs were 2.0 $\mu g \cdot L^{-1}$ and the LOQs were 5.0 $\mu g \cdot L^{-1}$. Table 4.2 summarizes analytical performances of various types of bismuth electrodes for the determination of cadmium (II) and lead (II) ions. The detection limits obtained from the Bi–CNT/GC electrodes for these two heavy metal ions are more or less in the same range with those of earlier literatures. Compared to the film and oxide screen printed electrodes [32,56], the detection limits of the Bi–CNT/GC electrodes were yet lower. In terms of the reproducibility, the standard deviations of 8 measurements for a solution containing 25 $\mu g \cdot L^{-1}$ of the metal ions were 2.44% and 3.19%, for cadmium (II) and lead (II) ion, respectively.

Compared to *in situ* BiF/CNT/GC electrodes (Section 4.3.4), the Bi–CNT/GC electrodes yielded higher sensitivity (slopes of calibration plots) for cadmium (II) and lead (II) ions. Nevertheless, the simple preparation and convenient operation of the Bi–CNT/GC electrodes have still brought the attention to continuously develop the Bi–CNT composite modified electrodes for the determination of heavy metal ions in real samples.

Table 4.2 Analytical performances of bismuth electrodes for the determination of cadmium (II) and lead (II) ions.

Electrodes	LODs ($\mu g \cdot L^{-1}$)		References
	Cadmium (II) Ion	Lead (II) Ion	
BiF/CNT/GC electrode	2.0	2.0	This work
Bi–CNT/GC electrode	2.0	2.0	This work
Polymer-coated BiF electrode	2.00	2.00	[20]
Bi/polyaniline film electrode	1.48	1.03	[21]
BiF-SPC electrode	8.00	10.00	[32]
BiF-CNT nanoelectrode array	0.04	0.04	[34]
Bi_2O_3-SPC electrode	16.00	8.00	[56]
Bi_2O_3-SPGC electrode	1.50	2.30	[57]

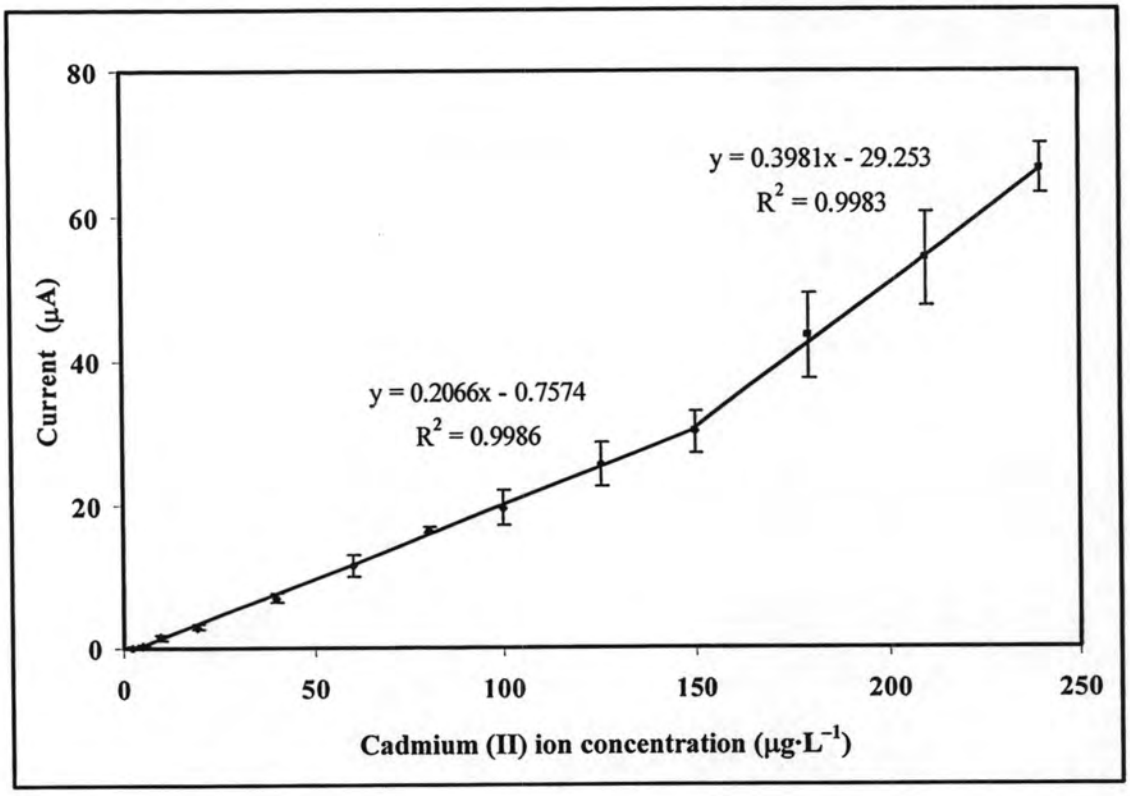

(a)

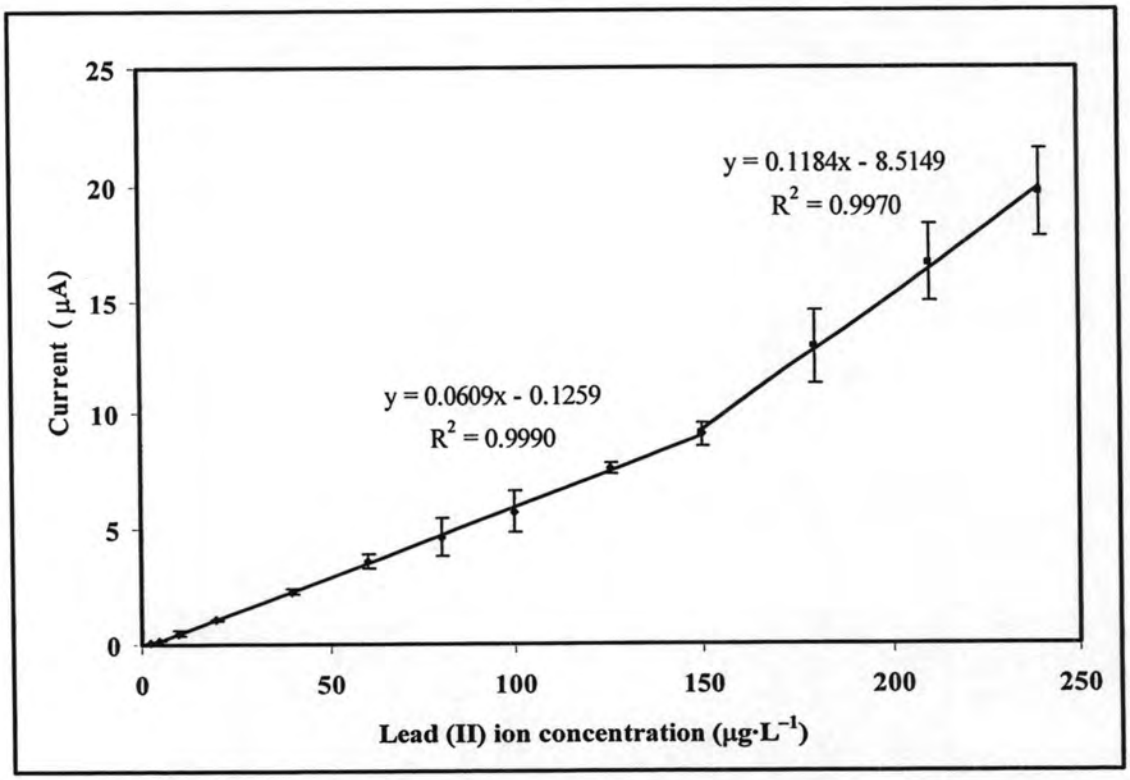

(b)

Figure 4.20 Calibration plots of (a) cadmium (II) and (b) lead (II) ions from SWASV analysis by 2.00 mol % Bi–CNT/GC electrodes in 0.1 M acetate buffer solutions using the same experimental conditions as those in Fig. 4.15.

4.4.5 Stability Studies of Bi–CNT Composite Modified Glassy Carbon (Bi–CNT/GC) Electrode

Since Bi–CNT/GC electrode had been developed for the detection of metals in real samples, its stability towards repetitive operation was probed. The amount of Nafion in the electrode was varied to adjust the electrode stability. After the preconcentration step at –1.10 V for 10 s, the SWAS voltammogram was recorded to yield the signals for cadmium (II) and lead (II) ions simultaneously by scanning the electrode potential from –1.10 V to –0.50 V. Due to the fact that –0.50 V is more negative than the oxidation potential of bismuth metal, electrochemical removal of bismuth particles on the electrode surface is technically protected. Then, the following measurement cycle was repetitively obtained. Fig. 4.21 shows repetitious SWASV analysis for a solution containing 100 $\mu g \cdot L^{-1}$ of cadmium (II) and lead (II) ions in 0.1 M acetate buffer solution (pH 4.5) by 2.00 mol % Bi–CNT/GC electrode with 0.50–2.00% Nafion solution. Using the stripping peak current obtained from the first measuring cycle as a reference, the plot of % peak current *versus* number of repetitive measurement is presented. The results exhibited that 2.00% Nafion provided the modified electrode with the best stability even though this Nafion quantity might not give the best sensitivity (Section 4.4.3.1). For cadmium (II) ion, the stripping peak current of the 2.00 mol % Bi–CNT/GC electrode with 2.00% Nafion (curve a of Fig. 4.21A) decreased significantly after the third use. For lead (II) ion, the current from the same type of electrode (curve a of Fig. 4.21B) began to change after the sixth use, implying that this Bi–CNT/GC electrode was more stable and effective towards the measurement of lead (II) ion. These results demonstrated that the Bi–CNT composite modified electrode could possibly be futher developed as a reusable and ready-to-use electrode for on-site screening purposes in conjunction with simple hand-held electroanalytical instrument.

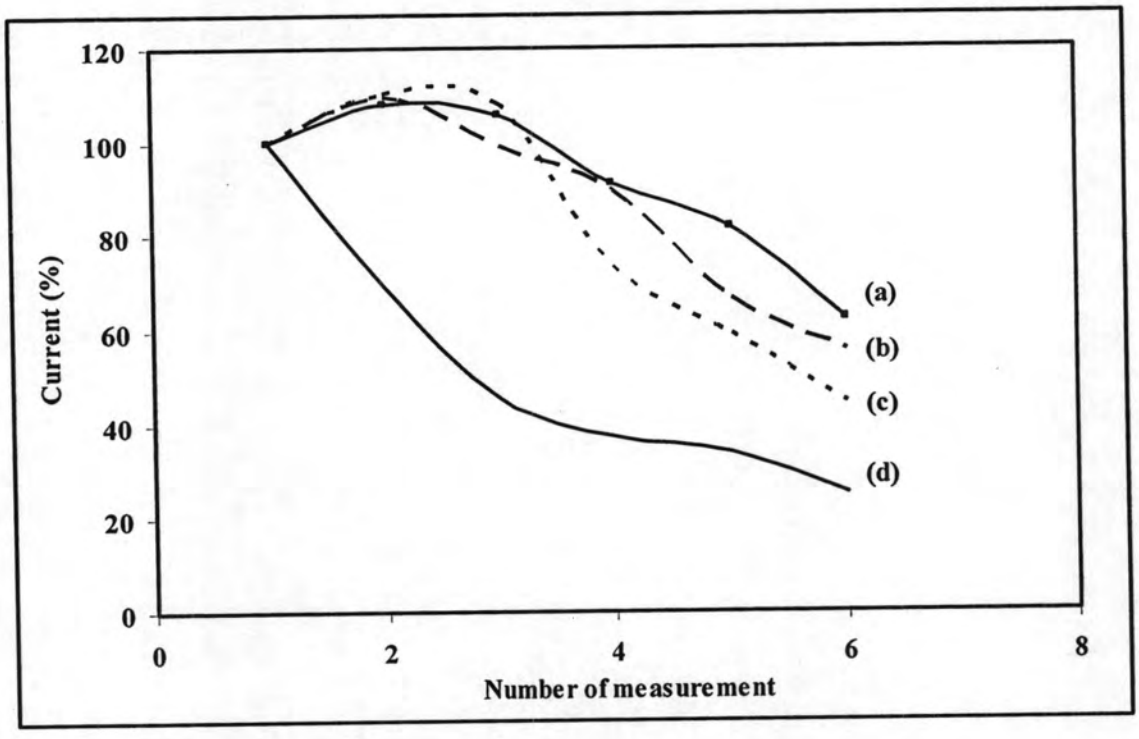

(A)

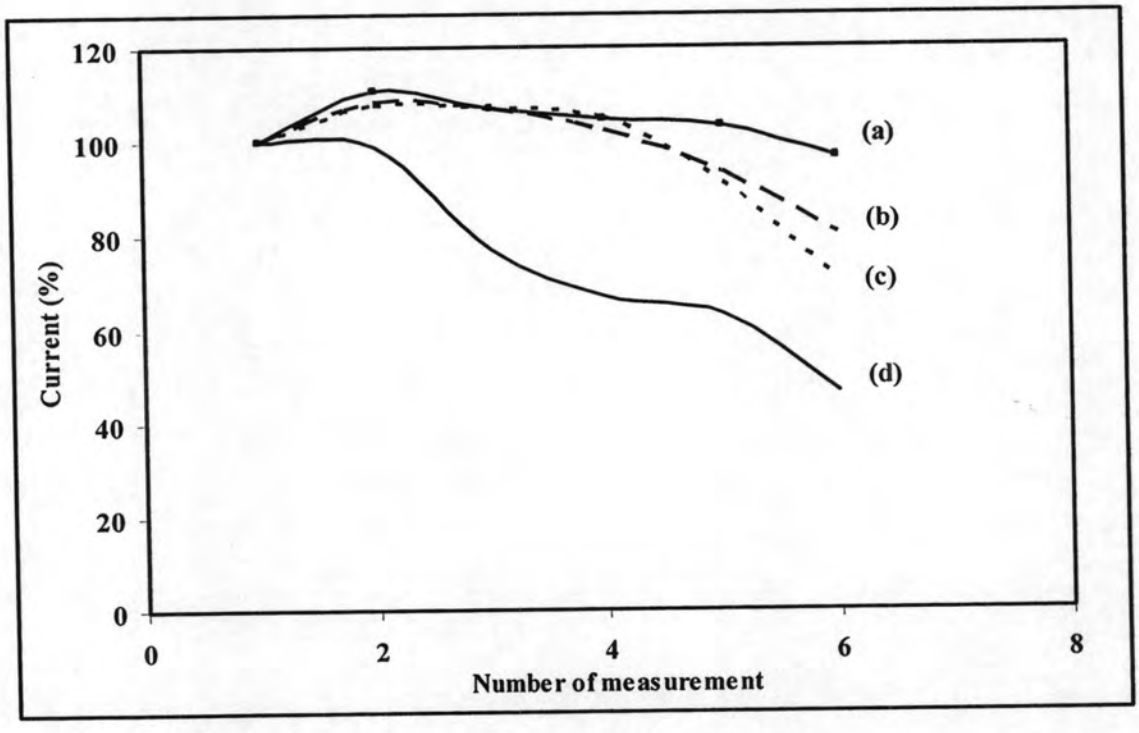

(B)

Figure 4.21 Stability studies of 2.00 mol % Bi–CNT/GC electrodes with (a) 2.00%, (b) 1.50%, (c) 1.00%, and (d) 0.50% Nafion for the determination of (A) cadmium (II) and (B) lead (II) ions by SWASV using the deposition potential of –1.10 V, the deposition time of 10 s, the stripping potential from –1.10 to –0.50 V, and the scan rate of 7.5 $mV \cdot s^{-1}$.

4.5 Determination of Cadmium (II) and Lead (II) Ion in Real Water Samples

In this section, the Bi–CNT/GC electrode and *in situ* BiF/CNT/GC electrode were comparatively tested for the determination of cadmium (II) and lead (II) ions in tap water and waste water samples. Table 4.2 exhibits the determined results obtained from the calibration curve method for both metal ions. Calibration curves in Fig. 4.13 and 4.20 were for *in situ* BiF/CNT/GC electrode and Bi–CNT/GC electrode, respectively. These electrochemical results were directly compared with data collected from inductively coupled plasma-atomic emission spectroscopy (ICP-AES), which was also used as a reference technique. Moreover, the Bi–CNT modified GC electrode was used for the determination of cadmium (II) and lead (II) ions in both water samples by the standard addition approach (Table 4.3).

Prior to SWASV measurement, tap water was mineralized with concentrated nitric acid (HNO_3) to remove some trace organic and inorganic species that might interfere the analysis. Being in good agreement with ICP-AES, the Bi–CNT/GC electrode found that there were 48.0 ± 1.6 $\mu g \cdot L^{-1}$ of lead (II) ions and none of cadmium (II) ion in tap water sample. On the contrary, the *in situ* BiF/CNT/GC electrode obtained higher concentration of lead (II) ion (84.6 ± 3.2 $\mu g \cdot L^{-1}$). This positive error might possibly arise from the earlier discovery that bismuth film electrodes were found to be sensitive towards strong acidic solution [21,58].

For the waste water sample, after wet digestion with concentrated HNO_3, the sample mixture was heated until dry and the remaining solid was diluted with 0.1 M acetate buffer to yield an appropriate sample solution for the analysis. At both electrodes, the amounts of lead (II) ions detected were different from the reference value, implying the issue of interference species. Since ICP-AES analysis found nickel (II) ions in the sample and earlier work revealed that the quantity of nickel (II) ion at 9-fold excess over lead (II) ion did suppress stripping peak of lead (II) ion [21], nickel (II) ion could be one interfering species in this case. For cadmium (II) ion, no data could be obtained since the remaining HNO_3 from sample digestion shifts hydrogen evolution positively until the cadmium stripping peak could not be seen on the Bi–CNT/GC and *in situ* BiF/CNT/GC electrodes.

Moreover, the results obtained without sample digestion were investigated. For both electrodes, the values of lead (II) ion quantities in undigested tab water were

much more than that of ICP-AES. It is likely that the matrix effect could affect the reliability of lead stripping signal.

Unlike the digested waste water, the undigested waste water could be used for the determination of cadmium (II) ion by SWASV using Bi–CNT/GC and *in situ* BiF/CNT/GC electrodes. However, the concentrations of both metal ions obtained from the electrodes were different from the ICP-AES data, implying the interference and matrix issues. It is possible that not only nickel (II) ion, but other metal ions or organic species might also have some impacts on the sensitivity of these bismuth electrodes. For example, previous work [21] reported that 5% signal was changed when the ratio of zinc (II) ion to lead (II) or cadmium (II) ions was 5.

Subsequently, in order to check whether the matrix effect was the cause of error, the Bi–CNT/GC electrode was employed for determination of cadmium (II) and lead (II) ions in tap water and waste water samples using standard addition method. Without any digestion treatment, both samples were adjusted to pH 4.5 with 0.1 M acetate buffer solution. After that, SWASV analyses were performed with the additions of cadmium (II) and lead (II) ion standard solutions. Determined results are shown in Table 4.3. For tap water, the metal concentrations obtained were in good agreement with the results found in ICP-AES measurement, revealing the existence of matrix issue in tap water. However, the concentrations of cadmium (II) and lead (II) ions in waste water sample analyzed by the Bi–CNT/GC electrode were lower than the results found in the reference method, indicating that the standard addition method could not resolve the detecting problem in waste water sample.

In summary, Bi–CNT/GC electrode was successfully applied to determine cadmium (II) and lead (II) ions in tap water by using either calibration curve method with the digested sample or standard addition approach with undigested sample. However, both Bi–CNT/GC and *in situ* BiF/CNT/GC electrodes could not be used to detect metal ions in waste water sample, possibly due to the matrix or interference issue. Therefore, due to simpler preparation and better electrochemical performance, various experimental parameters, especially the tolerance towards interferences or matrices, will be optimized to improve the ability of the Bi–CNT modified electrode for the metal determination in real samples.

Table 4.3 Determination results for tap water and waste water samples using calibration curve method.

Sample	ICP-AES ($\mu g \cdot L^{-1}$)		*In situ* BiF/CNT/GCE ($\mu g \cdot L^{-1}$)		Bi–CNT/GCE ($\mu g \cdot L^{-1}$)	
	Cadmium (II) ion	Lead (II) ion	Cadmium (II) ion	Lead (II) ion	Cadmium (II) ion	Lead (II) ion
Tap water[a]	N.D.	46.5 ± 2.1	N.D.	84.6 ± 3.2	N.D.	48.0 ± 1.6
Tap water[b]	-	-	N.D.	117.9 ± 2.0	N.D.	71.5 ± 6.1
Waste water[a]	13.0	34.5 ± 0.7	N.D.	40.4 ± 1.3	N.D.	28.8 ± 1.6
Waste water[b]	-	-	2.7 ± 0.2	33.1 ± 4.5	8.9 ± 0.1	40.8 ± 3.0

N.D. = not detected

[a] with HNO_3 digestion

[b] without HNO_3 digestion

Table 4.4 Determination results from SWASV analysis by Bi–CNT/GC electrode for tap water and waste water samples using standard addition method.

Sample[a]	Cadmium (II) ion ($\mu g \cdot L^{-1}$)	Lead (II) ion ($\mu g \cdot L^{-1}$)
Tap water	N.D.	47.3 ± 3.7
Waste water	4.5 ± 0.6	21.0 ± 1.5

N.D. = not detected

[a] without HNO_3 digestion